MAGNETIC RESONANCE IMAGING CONDITIONAL POWERED MICROINJECTOR FOR INTERVENTIONAL PROCEDURES

by

ADAM DAVID WINELAND

Under the Direction of

Zion Tsz Ho Tse

ABSTRACT

This thesis describes the development of a magnetic resonance (MR) conditional powered microinjector for use in clinical procedures and experiments taking place inside the magnetic resonance imaging (MRI) scanner. MR Safe devices pose no known hazards resulting from exposure to any MR environment, and they are composed of materials that are electrically nonconductive, nonmetallic, and nonmagnetic. Furthermore, equipment is considered MR Conditional if it poses no known hazards in a specified MRI environment within defined conditions, it does not significantly affect the image quality of the object being scanned, and its operation is not significantly affected by the MR environment. The core advantage of the MR Conditional microinjector is to accurately deliver therapeutics to subjects inside the scanner while reducing waste and inconsistent results which are created by using long transmission tubing between the scanner and an MR Unsafe injector located away from the MRI scanner or outside the MRI scanner room. This is particularly useful for expensive therapeutics such as stem cells.

The technical challenges of an MR Conditional microinjector include nonmagnetic actuation as well as high precision for control-release of the therapeutics. This is overcome by a custom-designed stepper motor based on pneumatic principles. The microinjector consists of three units: (1) a syringe actuator that contains a mechanism to precisely deliver therapeutics in a programmable volume or programmable pressure, (2) a pneumatic stepper motor, and (3) a software control panel that consists of a programmable interface for the user to set the volume or pressure of the delivery.

The presented microinjector has been validated in a 7 T MRI small bore scanner to ensure its usability in high-field MRI applications with less than 10 percent signal-to-noise ratio reduction in MRI images and with no image artifacts presented. Finally, the presented microinjector has been tested in a clinical proof-of-concept study to investigate the relationship between intraocular pressure and the tension in ocular tissue. The presented injector was utilized to adjust intraocular pressure of sheep eyeballs in vitro while the biomechanical response of the sclera was monitored by MRI and time-lapse photography.

The pneumatic-powered microinjector as well as the custom-designed pneumatic stepper motor alone could be utilized in a variety of MRI-guided applications. This project is in collaboration with the NeuroImaging Lab at the University of Pittsburgh.

INDEX WORDS: Magnetic Resonance Imaging, MR Conditional, Stepper Motor, Pneumatic, Geneva Drive, Microinjector, Glaucoma, Intraocular Pressure, Intact Globe Inflation Testing, Drug Delivery, Biomedical Devices

MAGNETIC RESONANCE IMAGING CONDITIONAL POWERED MICROINJECTOR FOR INTERVENTIONAL PROCEDURES

by

ADAM DAVID WINELAND

B. S., North Georgia College and State University, 2012

A or Thesis Submitted to the Graduate Faculty of The University of Georgia in Partial Fulfillment of the Requirements for the Degree

MASTER OF SCIENCE

ATHENS, GEORGIA

2016

MAGNETIC RESONANCE IMAGING CONDITIONAL POWERED MICROINJECTOR FOR INTERVENTIONAL PROCEDURES

by

ADAM DAVID WINELAND

Major Professor:	Zion Tsz Ho Tse
Committee:	Javad Mohammadpour
	Changying Li

Electronic Version Approved:

Suzanne Barbour
Dean of the Graduate School
The University of Georgia
August 2016

ACKNOWLEDGEMENTS

I would like to thank my classmates and colleagues Kengelle Chukwurah, Khushboo Brahmbhatt, Abhijit Marar, Yu Jiang, and Kenneth Ndyabawe for their insights and support. I would like to thank my current and former lab partners Dr. Stan Gregory, Alex Squires, Kevin Wu, Yabio Gao, Austin Taylor, Huawei Yang, Aleff Oliveira, and Yue Chen. It has been a pleasure getting to know all of you. I would like to thank my professors from classes I attended while at the University of Georgia: Dr. Mike Yoder, Dr. Tim Foutz, Dr. Phil Bartley, Dr. Jonathan Eggenschwiler, Dr. William Kissalita, Dr. Caner Kazanci, Dr. Charlie Li, Dr. Peter Kner, and Dr. K.C. Das. I thank Dr. Khan Hekmatyar for his knowledge and support during and after the MRI scans. I would like to express my gratitude toward Dr. Bill Tollner, Clodagh Phair-Miller, and Dr. Ramana Pidaparti for finding the funds that gave me a Teaching Assistantship during my graduate studies. I thank my coworkers Hillary Tanner and Dr. Ben Thomas for their support during and after my graduate career. I would like to thank my thesis committee members Dr. Javad Mohammadpour and Dr. Charlie Li for their support and suggestions. Lastly, I would to thank my advisor Dr. Zion Tse for accepting me into his lab and supporting my graduate studies.

TABLE OF CONTENTS

Page

LIST OF TABLES

Page

LIST OF FIGURES

Page

CHAPTER 1:

INTRODUCTION

1.1. Glaucoma

Glaucoma is the second leading cause of blindness with the first being cataracts. Several types of glaucoma exist with the two most common types being open-angle and angle-closure. Both kinds of glaucoma are caused by high pressure inside the eye. Figure 1.1 illustrates the basic anatomy of the human eye (a) and the two most common types of glaucoma (b, c). Open-angle glaucoma is a condition that develops slowly over time. As the name suggests, the angle of the eye is open, which is normal, but the drainage canals slowly become clogged at some point within the canals. Angle-closure glaucoma can develop quickly and is caused by a blockage at the entrance of the drainage canals [1].

The retinal ganglion cell (RGC) axons are responsible for passing information through the optic nerve head (ONH) to the brain. Over time, excessive intraocular pressure (IOP) causes blindness by inflicting irreversible damage to the RGC axons. Since the ONH is surrounded by the sclera, and the sclera transfers forces from IOP to the ONH at the scleral canal wall, researchers have developed experiments that are designed to study the biomechanics of the sclera [2].

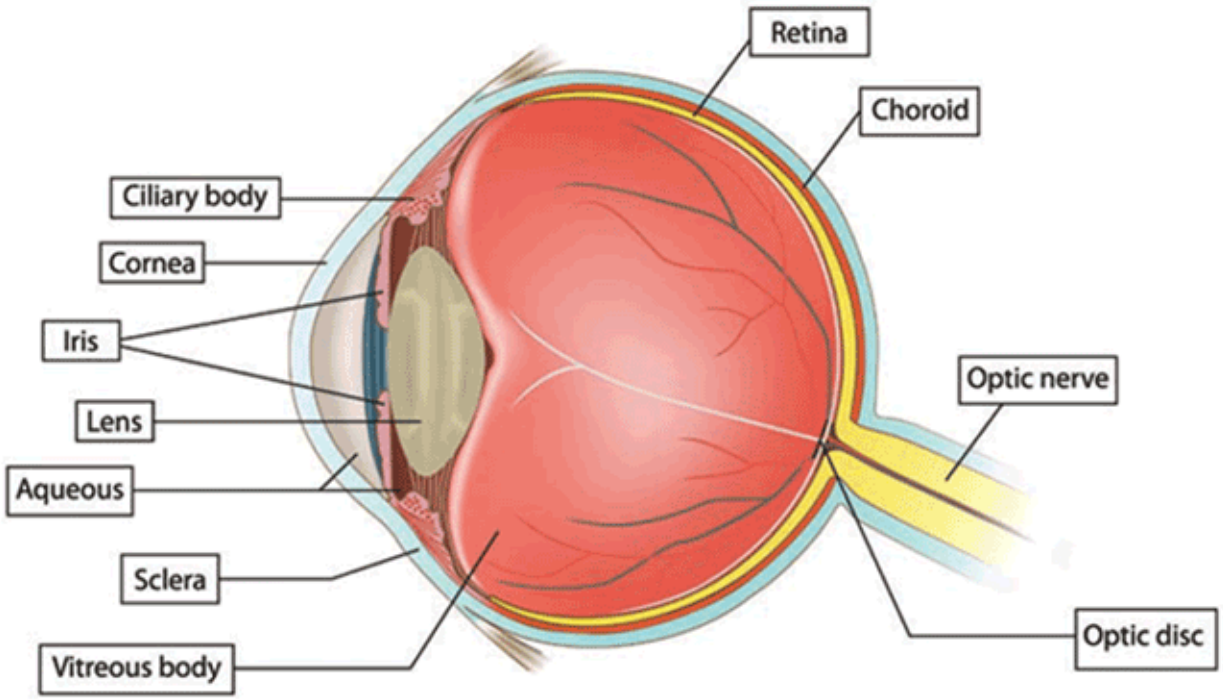

(a)

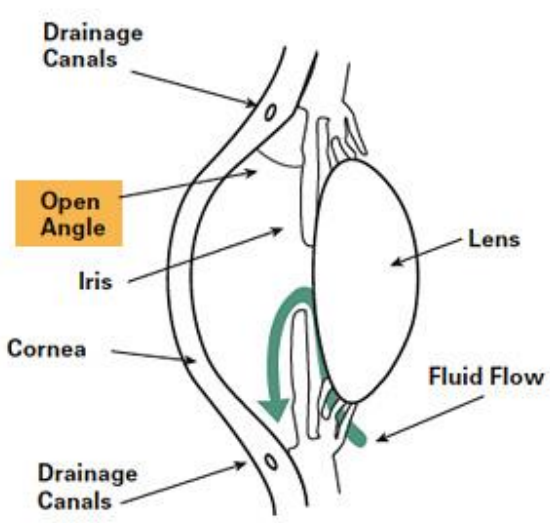

(b)

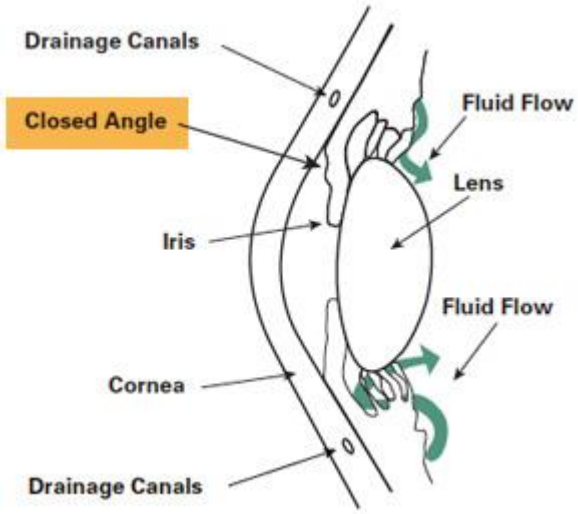

(c)

Figure 1.1: The basic anatomy of the human eye is displayed in the top image (a). Open-angle glaucoma (b) causes the drainage canals to clog slowly at some point inside the canal. Angle-closure glaucoma (c) occurs when the entrance of the drainage canals suddenly become clogged [1].

1.2. Inflation Testing

In an effort to study tissue deformation, several methods have been developed: uniaxial extension, biaxial extension, and inflation testing, to name a few. Uniaxial and biaxial tests involve excising strips of tissue and stretching the tissue using controlled stresses. Inflation tests involve inflating the corneoscleral shell of a donor eyeball in vitro using controlled pressurization while deformations of the shell are measured. Inflation tests can be performed on excised posterior scleral shells or on whole globes. Compared to excising strips of tissue, inflation testing better approximates the eye's normal biomechanical state [3].

Typically, the equipment required for inflation testing includes a fluid injection system, a container to hold the specimen, a humidity chamber, a device to measure displacement, and a device to measure thickness [3]. Figure 1.2 shows three different inflation systems used by researchers. Elsheikh *et al.* studied the modulus of elasticity of the human cornea using a custom pressure chamber to inflate excised corneas and charge-coupled device (CCD) cameras and a laser to measure changes in tissue. Coudrillier *et al.* used a syringe injection system to inflate excised posterior scleral shells and CCD cameras to monitor tissue changes. Ho *et al.* used a gravity perfusion system to inflate whole globes and magnetic resonance imaging (MRI) to study the effects of excessive IOP [4].

The average pressure in the human eye is relatively low (about 12 mmHg to 22 mmHg) [5] and pressure needs to be increased in small steps during experiments. The inflation systems used by Elsheikh *et al.* and Coudrillier *et al.* are capable of inflating an eye in small increments, but they are not compatible with an MR environment. On the other hand, the gravity perfusion system is safe to use in an MR environment, but it does not offer precise increments. Therefore, researchers are in need of a device capable of injecting liquid in small amounts while in the

vicinity of an MRI scanner. This thesis focuses only the first piece of equipment required for inflation testing: a fluid injection system. Specifically, research is focused on a programmable pump that increases pressure in small, precise increments by injecting distilled water or a saline solution into a specimen while operating in an MR environment.

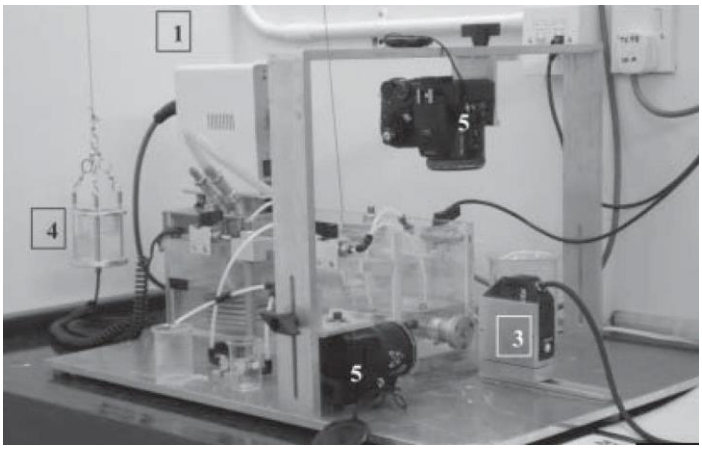

(a)

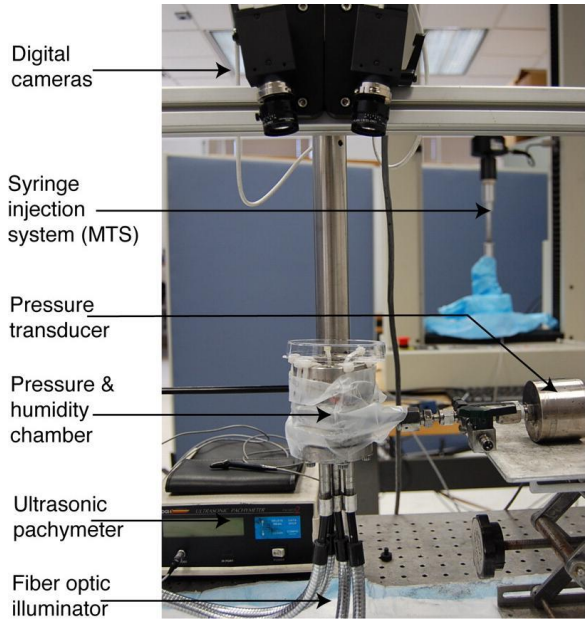

(b)

(c)

Figure 1.2: The top image (a) shows an inflation test system used by Elsheikh *et al.* [6]. On the bottom left (b) is a setup used by Coudrillier *et al.* [7]. On the bottom right (c) is a gravity perfusion system. The system used by Ho *et al.* would consist of all MR Safe or MR Conditional materials.

1.3. Microinjection

Conventional microinjection involves using a glass micropipette with a diameter of about 0.5 to 5 micrometers to inject small volumes of liquid, such as drugs or macromolecules, into a cell or other microscopic target [8]. Typically, the process is performed under a microscope while using two micromanipulators, devices which allow for small movements. One micromanipulator is used to position the target, and the other is used to maneuver the micropipette [9]. Figure 1.3 shows the conventional microinjection setup as viewed through a microscope. The microinjection process used in this thesis differs slightly from the conventional method; the device injects liquid into small areas instead of individual cells while viewing the specimen through MRI.

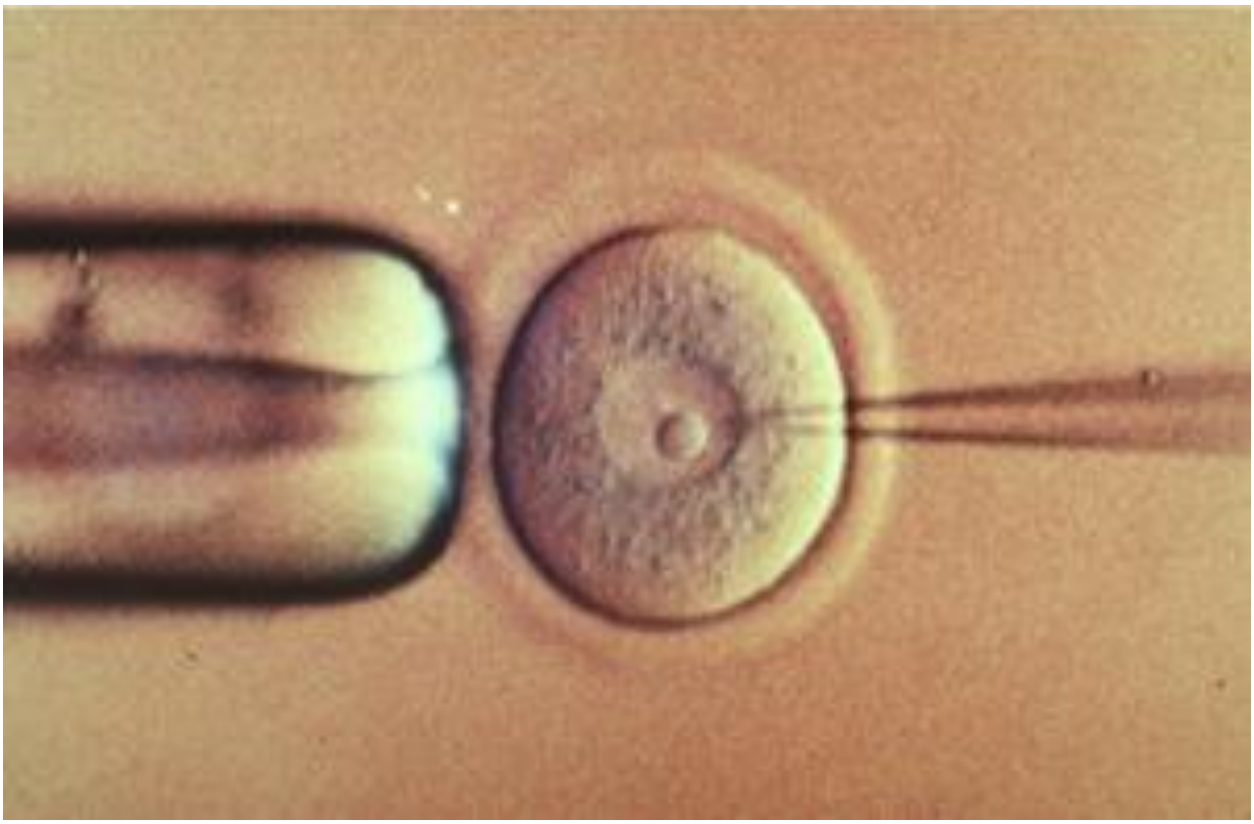

Figure 1.3: For conventional microinjection, one micromanipulator (left) holds the cell (center) while the micropipette (right) is inserted into the cell with a second micromanipulator [10].

Two types of microinjection systems exist: constant flow systems and pulsed flow systems. Constant flow systems deliver a continuous flow of fluid into a target. The amount of fluid injected depends on several factors: the amount of time the micropipette remains in the target, the pressure of the system, the viscosity of the liquid, and the diameter of the pipette opening. Pulsed flow systems inject fluid in precise increments allowing for more consistent results, but these systems are usually more expensive [11]. Microinjectors are further divided into analog and digital subcategories. The tubing extending from the microinjector to the micropipette holder is filled with oil, distilled water, or air depending on the design of injector. Only the micropipette is filled with the fluid or substance to be injected. For analog microinjectors, the fluid is released from the micropipette by rotating the knob on the rear of the microinjector base. Some digital microinjectors use a foot pedal to activate the injection while others can be activated with a button attached to the microinjection system. Hydraulic microinjectors typically offer more consistent results because of the incompressible medium transferring the force of the rotated knob to the substance inside the micropipette. However, they are prone to air bubbles and messy maintenance due to the oil or water. Pneumatic microinjectors offer a clean and virtually maintenance-free option, but the benefits come at a cost due to the precision machining and calculations of the components. Figure 1.4 shows some different types of microinjectors

(a)

(b)

(c)

(d)

Figure 1.4: Above are examples of commercially available injectors. The Narishige IM-6 (a) [12] is an analog oil-based microinjector. The Narishige IM-11-2 (b) [13] is an analog pneumatic microinjector. Both the Tritech MINJ-D (c) [14] and Eppendorf Femtojet 4i (d) are digital pneumatic microinjectors [15].

Microinjection is often used to inject a single cell with genetic material. Microinjection is used for genetic engineering and research, cloning, and cell biology studies. Other applications include intracytoplasmic sperm injection, in vitro fertilization, stereotactic surgery, stem cell therapy, retinal pigment epithelial, and intraocular injection. These practices, particularly the ophthalmology procedures, are further enhanced by using MRI to guide the operator and monitor changes in tissue. However, the technique for MRI-guided microinjection is different from the conventional definition. In place of a microscope is an MRI scanner, thus individual cells cannot be targeted for injection since a cell requires high magnification to be viewed. Instead, small areas of the specimen are targeted, and fluid is injected in minute quantities.

Despite the multiple applications of microinjection, the scope of this thesis involves injecting small volumes of fluid into a donor eyeball in vitro while measuring the pressure inside the system and monitoring deformations of ocular tissue.

1.4. Magnetic Resonance Imaging

Magnetic resonance imaging (MRI) is capable of acquiring high resolution images of soft tissue. The technique is most valuable for preoperative and intraoperative medical procedures [16]. Additionally, MRI is capable of revealing delicate changes within the target of interest without invading the sample, thus making it useful for researching the internal anatomy of a specimen. The process does not utilize nephrotoxic contrast agents or ionizing radiation found in X-rays (radiographs) and Computed Tomography (CT). Instead, images are acquired by using static magnetic fields and radiofrequency pulses.

MRI guided robotic therapy has drawn increasing attention due to its ability to provide accurate, efficient, and safe operation inside the MRI room. However, few components for robotic actuation near the MRI scanner are available because the magnetic field of the scanner precludes the use of traditional actuators fabricated with ferromagnetic or paramagnetic materials, such as DC stepper motors. These devices are prone to produce their own magnetic field and affect the homogeneity of both the static and gradient magnetic fields of the MRI scanner resulting in image artifacts. The interference is not one-sided; functionality of traditional robotic components is affected by the powerful magnet of the MRI scanner. Furthermore, ferromagnetic objects have the potential to become deadly projectiles the closer they come to the MRI machine. Therefore, the development of additional MR Conditional actuators is desired to deliver safe, reliable robotic operation while ensuring the quality of images.

The MR Conditional actuation methods can be divided into three categories according to the MR safety of the device: intrinsically MR Conditional actuators (e.g. pneumatic principle), electric actuators (e.g. piezoelectric technology), and electromagnetic actuators [17]. Piezoelectric materials are considered MR Conditional, but electric energy required to operate these materials is carried into the room of the MRI scanner. Thus, electromagnetic interference (EMI) is emitted and therefore causes a decrease in the quality of MR images [18, 19]. Electromagnetic actuators with permanent magnets should be shielded and placed at a safe distance from the scanner [17].

Unlike electric and electromagnetic actuators, pneumatic devices exhibit a few advantages inside the MRI room. They can be made out of MR Safe materials, such as plastic, which are readily available, easy to machine, and cost-effective. Pneumatic devices operate on compressed air which is available in most MRI control rooms. In addition, the compressed air

does not affect the magnetic field or image quality. Pneumatic actuators introduce an insignificant reduction to the signal-to-noise ratio (SNR). These advantages result in the fast development of pneumatic actuation for MRI-guided robotic interventions [20, 21].

1.5. Thesis Contributions

The field of MRI is young and growing rapidly. MRI-guided surgery is considerably younger, but it is a promising area of interest in need of accurate, reliable tools. Only a handful of pneumatic stepper motors have been developed for the field, and none have reached commercial status. Thus, the pneumatic stepper motor developed in this thesis is an important contribution to the limited number of MR Conditional actuators because of its unique approach.

In this thesis, the microinjector is tested to prove its efficacy in inflating and pressurizing eyeballs while in an MR environment. These tests help researchers study IOP and its connection to glaucoma. However, the microinjector can be utilized in numerous MR-guided applications such as stereotactic surgery, drug infusion, and stem cell therapy. Similarly to the pneumatic stepper motor, few commercially available MR-compatible syringe pumps exist, but their proximity to the MRI scanner is limited. The microinjector discussed in this thesis is capable of being placed directly in front of the bore of the MRI scanner, significantly reducing the length of tubing required for experiments and surgery.

1.6. Brief Overview of the Thesis Organization

This thesis is divided into two main components. First, the development of an MR Conditional pneumatic stepping device is described in Chapter 2. The design and working

principle of the motor is explained in detail, and its performance is evaluated with respect to torque, speed, and accuracy.

The second part of the thesis, Chapter 3, describes the development of an MR Conditional microinjector utilizing the aforementioned stepping device. The working principle and control software are described in detail. Performance of the microinjector is evaluated by inflating an eyeball and recording the progression of inflation with a camera and MRI while monitoring system pressure. The compatibility of the microinjector in an MR environment is also evaluated.

Chapter 4 offers a summary of the thesis and ideas for future optimizations and applications.

CHAPTER 2

DEVELOPMENT OF AN MR CONDITIONAL ACTUATOR

2.1. Background and Preliminary Studies

In order to provide precise actuations or manipulations in the surgical diagnosis, such as needle biopsy [17] or radiation treatment, a couple of approaches have been applied to MR Conditional actuators [22]. One method studied by several research groups is to apply different control strategies to the actuators such as PID control [23] and sliding mode control [24]. However, the extra instruments introduced to the MR room to integrate with the actuator, such as sensors and encoders, are generally not compatible with the MR environment. In contrast to using extraneous equipment and complex algorithms, a stepper actuator operates with accurate, discrete steps and thus achieves the precision necessitated by the surgical operations.

Several MR Conditional pneumatic stepper motor designs generally rely on the intermeshing of different sets of "teeth" to create the rotation and stepwise effect. Stoianovici *et al.* created a pneumatic stepper motor called PneuStep which uses three diaphragm mechanisms to rotate a central toothed gear (Figure 2.1a) [21]. Chen *et al.* designed a pneumatic stepper motor that does not rely on the intermeshing of teeth (Figure 2.1b) [25]. Instead, two pneumatic cylinders operate in sequence to rotate a shaft in discrete steps. This process is similar to that of a two-stroke engine. Sajima *et al.* developed a pneumatic stepper motor that alternates the extension and retraction of three pistons with teeth to push on the face of a central toothed gear (Figure 2.1c) [20]. Compared to the PneuStep motor, this motor has fewer components and is smaller in size. Chen *et al.* designed a second pneumatic stepper motor with a diameter of 10

mm, which is significantly smaller than Stoianovici's and Sajima's (Figure 2.1d) [26]. This motor uses two push rods and interlocking teeth to create a stepped rotation but only in one direction. Wei *et al.* developed a pneumatic motor that blows compressed air onto a blade of a fan structure (Figure 2.1e) [27]. Stepping motion and continuous motion are achieved by implementing a roller valve into the base of the device and controlling the air pressure applied to the roller valve.

The pneumatic stepper motor presented in this thesis utilizes a Geneva drive to achieve stepping motion, specifically, an external Geneva drive. Several variations of continuous-to-intermittent mechanisms and gear combinations exist. These devices, also known as indexing mechanisms, convert the continuous rotation of a gear or shaft into discrete steps. However, the challenge with developing a stepper motor does not lie solely on creating stepped motion out of continuous input. Instead, the challenge is being able to stop the continuous motion in between steps. To accomplish this task, the Geneva drive was chosen because of its long dwell period, the time between steps. Another factor involved in the decision of an indexing mechanism for a stepper motor is the ability to lock the output gear during the dwell period. Locked output is intrinsic for the Geneva drive. Strictly speaking, the slotted gear is locked in place by the pinned gear's stop disc, the part that resembles a crescent moon, when the pin is not interacting with the slotted gear. As a bonus, the compactness of the Geneva drive allows for a small footprint of the overall assembly of the motor. Figure 2.2 illustrates the components of a typical Geneva drive.

(a)

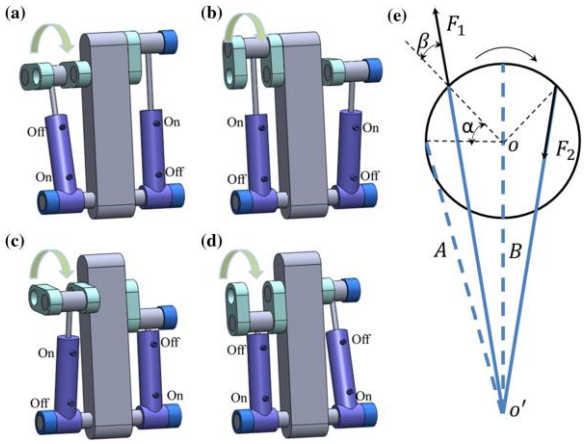

(b)

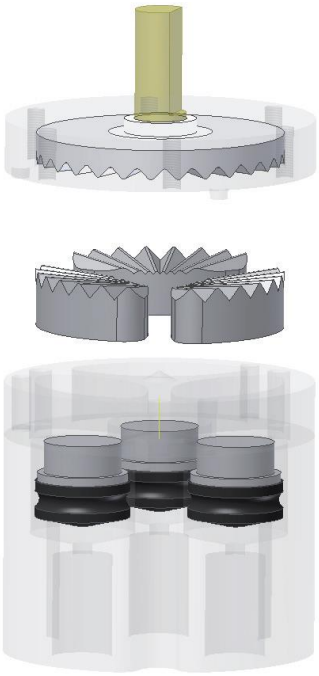

(c)

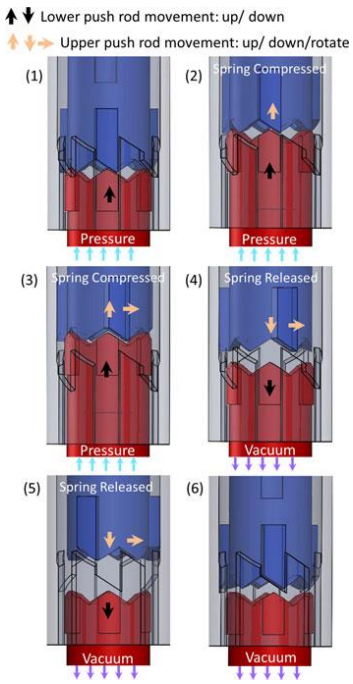

(d)

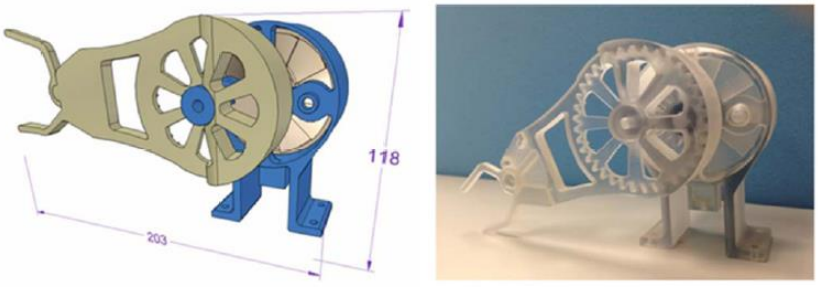

(e)

Figure 2.1: Stoianovici PneuStep motor (a), Chen dual cylinder motor (b), Chen 10 mm unidirectional motor (c), Sajima MR Safe Pneumatic Rotation Stepping Actuator (d), Wei fan structure motor (e)

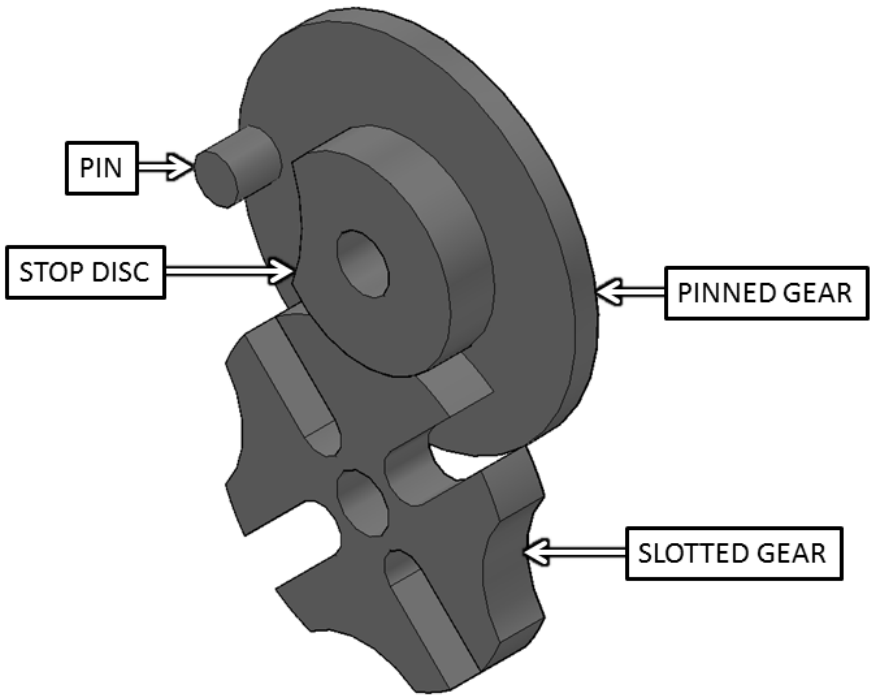

Figure 2.2: The components of a typical Geneva drive

2.2. Assembly of Pneumatic Stepper Motor

Figure 2.3 shows the main components of the stepper motor which include a continuous pneumatic motor with planetary gearbox, two pneumatic switches, two pneumatic cylinders, a Geneva drive, and a chassis. The continuous pneumatic motor with planetary gearbox is attached to the outside of the chassis. The planetary gearbox is required to produce the torque necessary to close the pneumatic switches. Inside the chassis are the two pneumatic cylinders, which are attached to the pneumatic switches, a cam to push the switches closed, and a Geneva drive. Opposite of the continuous motor is a second planetary gearbox to improve torque and stepping resolution. The planetary gearboxes are produced by Tamiya (Part number: 72001, Tamiya America, Inc., Irvine, CA, USA). The pneumatic switches and cylinders are produced by Lego (Part numbers: 47223 and 74981, respectively, Lego Group, Billund, Denmark). The chassis, continuous motor, and Geneva drive are custom-built. All components were fabricated from acrylonitrile butadiene styrene (ABS), nylon, brass, polylactic acid (PLA), or photoreactive resin to ensure they are compatible with the MR environment. The switches were modified by drilling the ports to a larger diameter thus allowing for greater air flow.

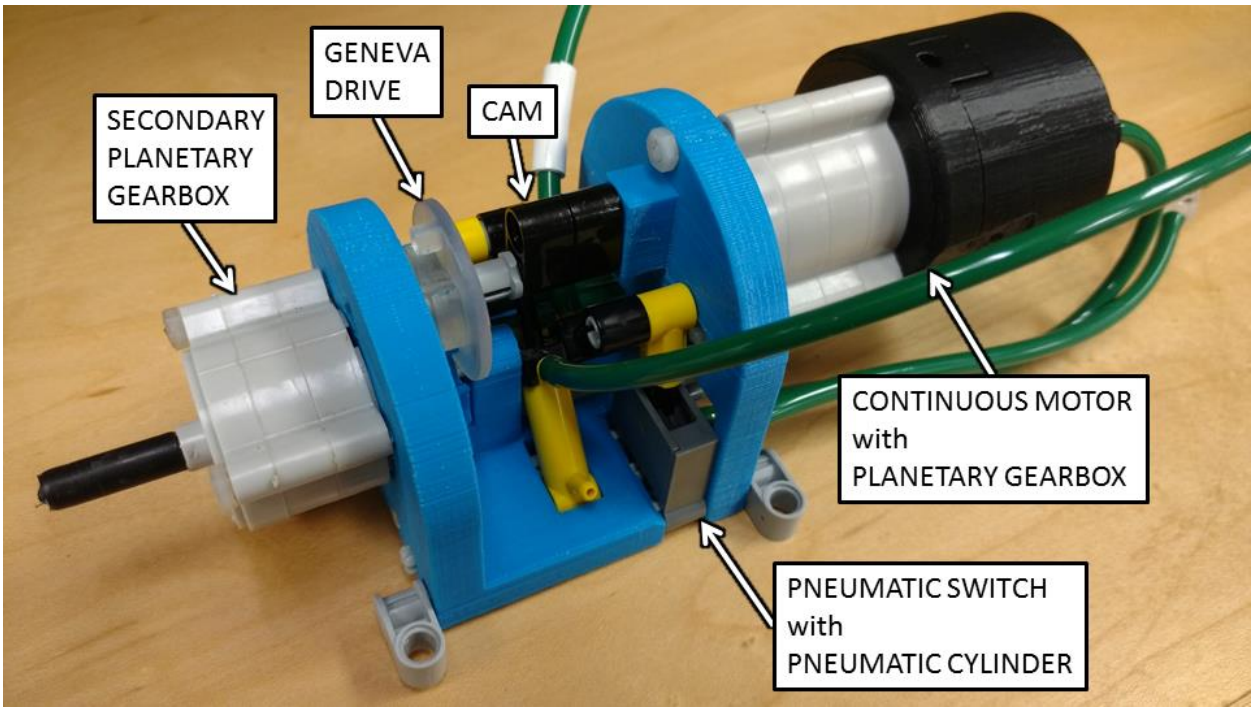

Figure 2.3: To the right of the chassis is a continuous pneumatic motor with a planetary gearbox. Inside the chassis are a cam, two Lego pneumatic switches, two Lego pneumatic cylinders, and a Geneva drive. To the left of the chassis is a second planetary gearbox.

2.3. Control Electronics and Software

The control electronics involve a data acquisition (DAQ) card (USB-6009, National Instruments, Austin, TX, USA), a valve driver circuit (Compact L298 Motor Driver, Solarbotics Ltd., Calgary, Alberta, Canada), and two 3-way solenoid valves (3AK-1/8-G, WIC Valve, Silicon Valley, CA, USA). LabVIEW is used to interface with the DAQ card. All components are powered by a 12 VDC power supply.

The software is based on pulse-width modulation (PWM), but it operates at a much simpler and slower scale than typical PWM applications. Each period corresponds to one step, and the frequency is considered as the number of steps per second. The high signal of a period relates to the amount of time a solenoid valve is open, allowing air to flow to a pneumatic cylinder and retract it. The low signal relates to the amount of time the valve is closed, releasing

the pressurized air trapped between the valve and cylinder. Initial tests concluded that 500 ms is required for the time high regardless of period length. This amount of time allows enough air to flow through and pressurize the long pneumatic tubing so that the cylinder retracts properly.

2.4. Working Principle

Figure 2.4 is a block diagram of how the stepper motor operates. Figure 2.5 illustrates the mechanical working principle of the stepper motor. First, a supply of compressed air is directed to both the control box and the motor assembly. Inside the control box, the air enters the solenoid valves. Each valve corresponds to one of the pneumatic cylinders inside the stepper motor chassis. The valves are activated by digital signals from the DAQ card. One of the digital outputs controls clockwise rotation, and the other output controls counterclockwise rotation. The signals from the DAQ card must first enter the valve driver circuit which provides the current required to open the valves.

When a digital high signal is sent to one of the valves, the valve opens allowing air to flow to the corresponding cylinder, and the cylinder retracts and pulls its connected switch to the open position. Air then flows through the switch and to the continuous motor. The continuous motor rotates either clockwise or counterclockwise (depending on which switch was opened), rotating the cam and Geneva pinned gear in unison. The cam is designed to reset the switch and cylinder to their initial positions by pushing on them. However, before the cam makes contact with the switch and cylinder, the DAQ card sends a digital low to the same valve, exhausting the air trapped in the tubing between the cylinder and valve. This allows the cam to push the switch and cylinder with less resistance. Once the switch is reset, the air flow to the continuous motor stops, quickly halting rotation of the cam and Geneva pinned gear. The motor is now ready for

another signal for either direction. For each rotation of the cam, the pin has rotated once as well. And for each rotation of the pin, the Geneva slotted gear has rotated a quarter of a rotation, or one step, because it has four slots. In essence, the stepper motor advances one step and turns itself off for every signal pulse.

After the Geneva slotted gear has advanced one step, it is unable to rotate because of the Geneva drive's inherent design. The Geneva drive alone delivers a stepping resolution of 90 degrees. The aforementioned second planetary gearbox connected to the chassis (shown in Figure 2.3) is attached to the output of the slotted gear. The ratio of this gearbox is 25:1 thus improving the stepping resolution from 90 degrees to 3.6 degrees.

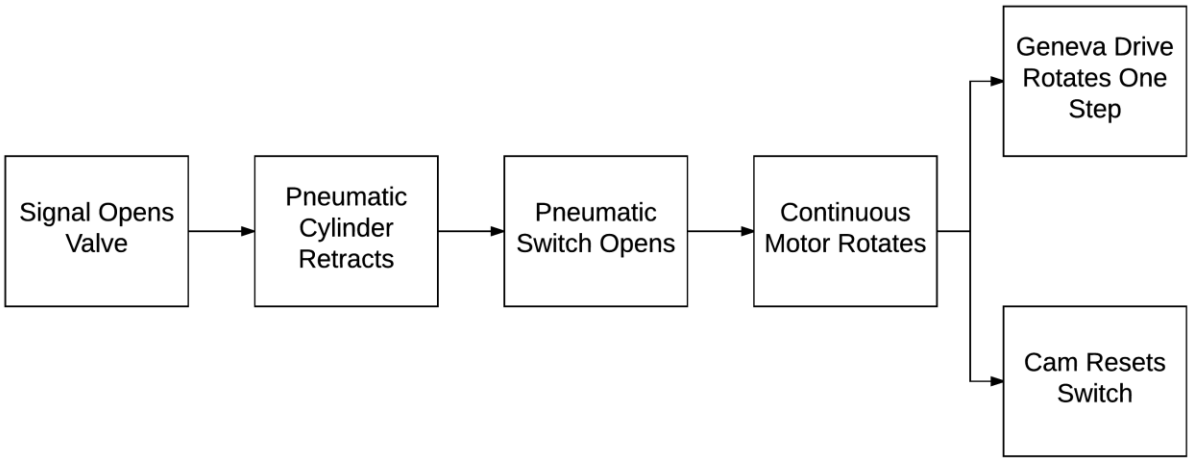

Figure 2.4: Block diagram of stepper motor working principle

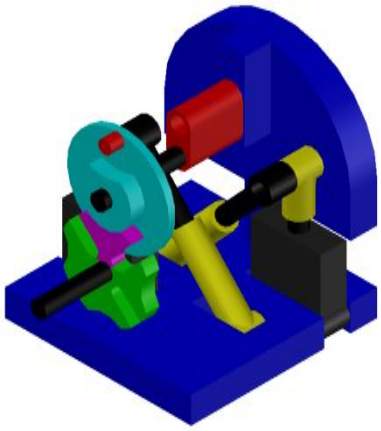

(a) The system is ready for a signal.

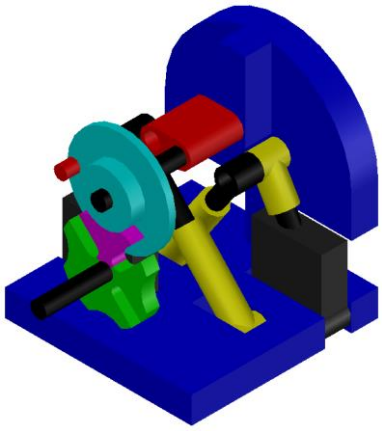

(b) A signal opens a valve in the control box, and the corresponding pneumatic cylinder retracts and pulls its switch to the open position. With the switch open, the continuous motor rotates the Geneva pinned gear counterclockwise.

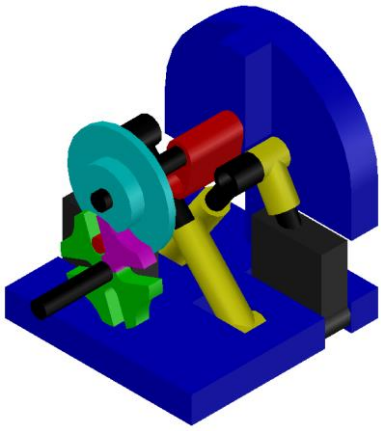

(c) The cam on the main shaft begins pushing the switch to the closed position. The pin on the Geneva pinned gear meshes with the slotted gear, rotating the slotted gear clockwise.

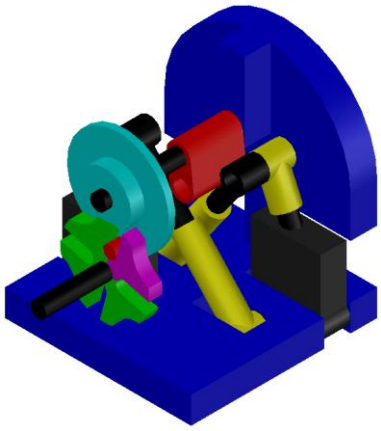

(d) The cam has almost finished pushing the switch closed. The pin is exiting the slotted gear.

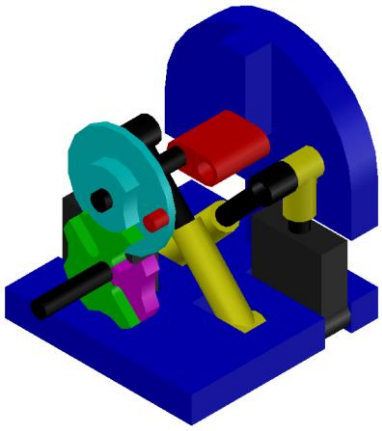

(e) The pin has exited the slotted gear, and the switch is closed. The main shaft is slowing to a stop.

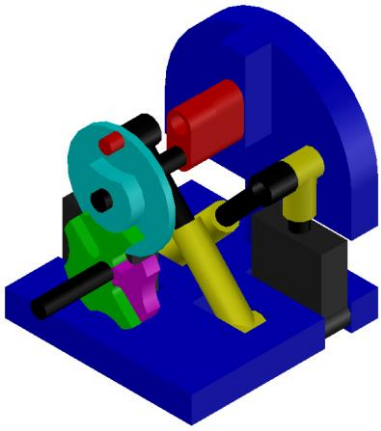

(f) The main shaft has stopped, and the system is ready for another signal.

Figure 2.5: The mechanical working principle of the stepper motor for a clockwise rotation of the slotted gear (counterclockwise rotation of the pinned gear and cam)

2.5. Experimental Setup

The motor's torque was measured against selected input pressures and operating speeds. The accuracy of the motor was tested against chosen operating speeds at 50 psi. Operation of the motor is defined as making the motor's cam (the part that flips the switches to the off position) start and stop within 15 degrees of vertical after one rotation. Overshoot for this motor does not refer to the output of the final planetary gearbox; overshoot refers to the cam stopping beyond the designated range (15 degrees of vertical). Alternatively, undershoot refers to the cam stopping before the designated range. This method ensures that the motor does not stall when it is operated in the opposite direction. Operating pressure is dependent on the length of tubing from the regulator to the device. For this experiment, pneumatic tubing with a length of 10 feet and inside diameter of 0.15625 (5/32) inches was used for each of the three lines extending from the control box to the stepper motor (one line for each pneumatic cylinder and one for the continuous motor).

Minimum and maximum loads were determined directly from the Geneva slotted gear (without the final planetary gearboxes attached) for chosen pressures in order to reduce the number of required weights. In addition, the maximum operating speed was found with respect to the minimum and maximum loads for each pressure. To determine maximum loads, a basket to hold weights was attached to an offset axle with a 1:1 pulley system [28]. Then the motor was operated continuously at a specified rotational speed. The cam was closely monitored for stopping within the designated range. If the cam landed within the desired range for several steps, another weight was added. If the cam did not stop within the designated range, then the previous value of the load was considered the maximum.

2.6. Test Results

At 40 psi and below, the pressure is too low, and the cylinders did not retract. With input pressure set to 50 psi and no load attached to the pulley, the motor is capable of operating at 144 degrees per second. Assuming the 25:1 planetary gearbox is attached, the rotational speed is ω = 144 deg/sec ÷ 25 = 5.76 deg/sec. The motor is able to lift up to a maximum of 4N, or 100N with the planetary gearbox attached. At 4 N, the fastest the motor can operate is 108 deg/sec, or 4.32 deg/sec with the planetary gearbox while lifting a load of 100 N. The radius of the Lego axle rod is 2.45 mm. So the maximum torque produced by the Geneva drive is T_{Geneva} = 4 N × 2.45 mm = 9.8 mN·m. And with the 25:1 planetary gearbox attached to the Geneva slotted gear, the final torque is T_{final} = 9.8 mN·m × 25 = 245 mN·m.

At 60 psi and no load attached, the cam achieves a stopping position closer to vertical compared to 50 psi. The maximum rotational speed with no load is 153 deg/sec (6.12 deg/sec). The maximum load is 15 N (375 N), so the maximum torque is T_{Geneva} = 15 N × 2.45 mm = 36.75 mN·m, or T_{final} = 36.75 mN·m × 25 = 918.75mN·m. At maximum load, the motor is capable of operating at 135 deg/sec (5.4 deg/sec).

At 70 psi, a minimum load of 29 N (725 N) is required to prevent overshoot. The minimum load just so happens to be the near the maximum load for the pin on the Geneva pinned gear. That is, the pin broke off at around 34 N (850 N). After replacing the Geneva pinned gear, the motor was tested at 80 psi. Unfortunately, the pin broke off again before an initial load could be determined.

Figure 2.6 shows the relationship between rotational speed and load with the planetary gearbox attached. The shaded area denotes acceptable operating conditions for 50 psi and 60 psi. For example, at 50 psi, the motor is capable of moving a load of 100 N at any rate from 0 deg/sec

up to 4.32 deg/sec. Conversely, if a speed of 5 deg/sec is desired, the motor can move any load from 0 N up to about 50 N.

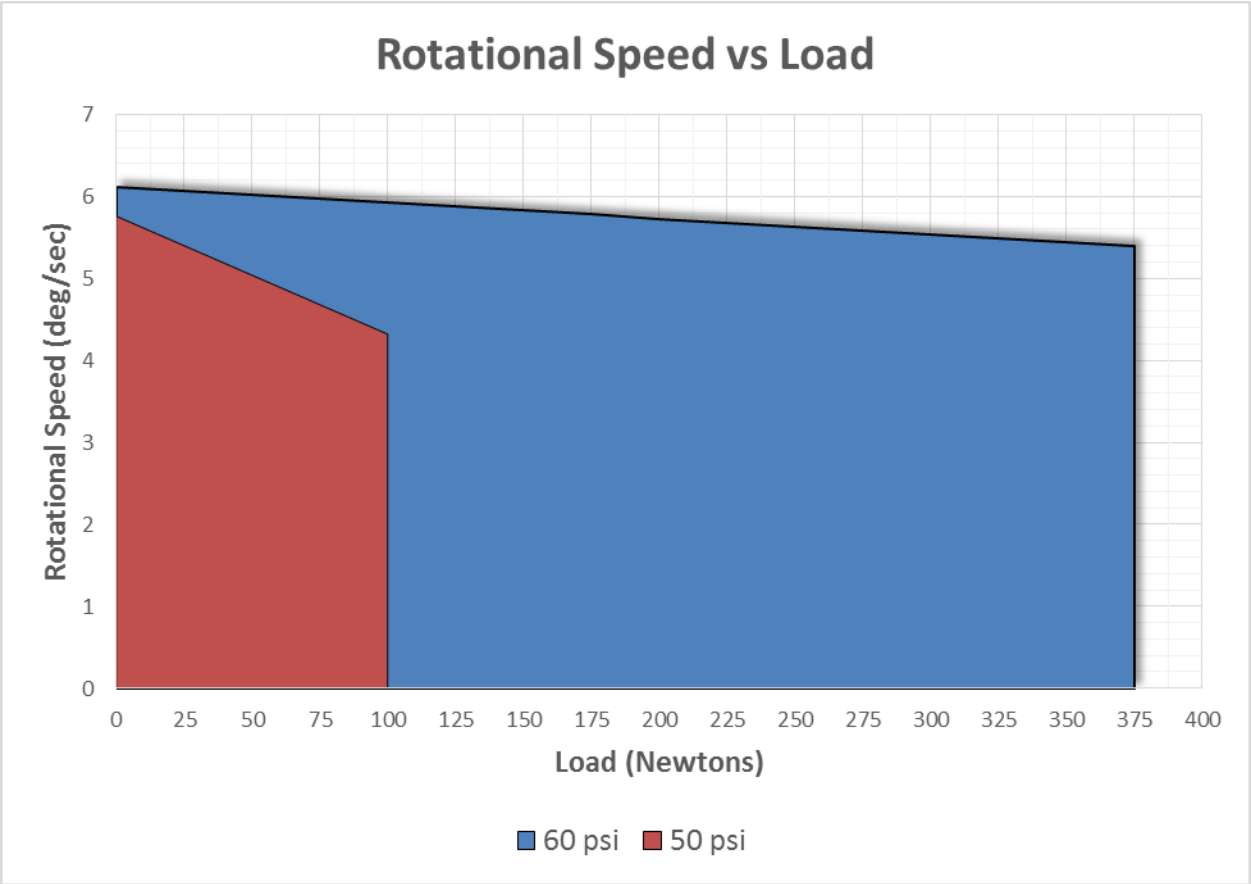

Figure 2.6: The graph shows the relationship between load and rotational speed for 60 psi and 50 psi. The shaded areas denote the optimal operating conditions for each pressure [29].

The accuracy of the motor with the 25:1 planetary gearbox was determined by using a rotary encoder (E6C2-CWZ3E 1024 P/R, Karlsson Robotics, Jupiter, FL, USA) attached to the end of the output shaft. Accuracy is independent of the load because, under proper operating conditions, the Geneva drive either completes a step or it fails. Also, the Geneva drive's design renders each subsequent error independent of the previous error. In other words, the Geneva slotted gear is held in place after each step, and the cam will achieve a near vertical position if

the device is operated within optimal load and timing limits. Therefore, overshoot and undershoot as defined in section 2.5 have no effect on the final output. Instead, accuracy is mainly dependent on the machining tolerance of the Geneva drive. Figure 2.7 shows the motor's average angular error versus different target angles at 60 psi with no load for different operating speeds. Target angles chosen are multiples of the motor's resolution, which is 3.6 degrees. The angular error is defined as the difference between the encoder's measured value and the desired target angle. The average angular error is calculated by taking the statistical mean of five sampling values.

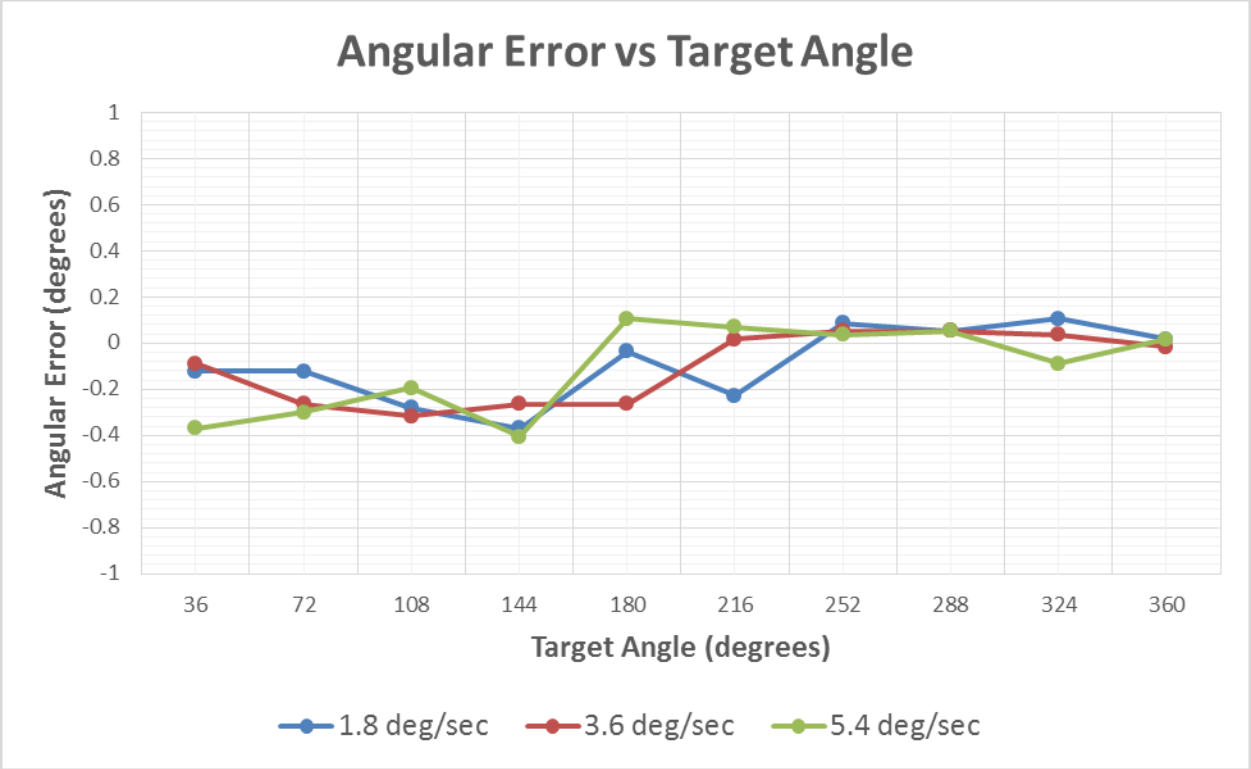

Figure 2.7: The graph shows the relationship between target angle and accuracy. Each line represents a different rotational speed. Each data point represents the mean of five sampling values.

2.7. Conclusions

The components that make up the stepper motor are readily available, inexpensive, and easy to manufacture. The control hardware and software are simplistic in design. The duration of the Geneva drive's dwell period allows the inertia of the cam to become zero before the pinned gear interacts with another slot in the slotted gear. When the cam and pinned gear stop, the motor is ready for another signal to retract a cylinder and repeat the process.

The optimal pressure for this design and setup of the stepper motor is 60 psi, and the maximum operating speed is 5.4 deg/sec with a maximum load of 15 N. The motor's stepping resolution is 3.6 degrees, accurate to within 0.5 degrees of the target angle, and accuracy is independent of operating speed if operating at maximum speed or below. The motor generates up to 918.75 mN·m of torque. Operating the motor at pressures higher than 60 psi increases the speed and torque of the motor but at a cost: the output must have an initial load attached in order to prevent the cam from overshooting and stalling the motor. And too much torque causes the pin to snap off of the driving gear. Any pressure below 50 psi does not power the motor.

2.8. Future Work

Future work involves increasing the motor's rotational speed and developing a smaller physical profile. Optimizing parameters such as the input pressure and planetary gear ratio will allow the motor to complete more steps per second. Custom switches designed to be smaller and less resistant will allow for a lower input pressure and gear ratio. Future pinned gears will be fabricated to be more robust so that the pin does not break as easily. Thus, operation at pressures higher than 60 psi can be investigated. Operating the motor at lower pressures is also a possibility if the amount of flow is increased by means of larger inner-diameter tubing. Wider

tubing will also allow for longer air supply lines. Despite an already low angular error, accuracy could be further improved by machining the Geneva drive to tighter tolerances

The most significant outcome of this project is the switch box, which is the chassis and its internal components, since it is able to turn continuous motion into intermittent motion. In other words, the switch box could be adapted to work with any hydraulic or electric continuous motor. Future research also involves experimenting with other indexing gears and continuous-to-intermittent mechanisms.

CHAPTER 3

DEVELOPMENT OF AN MR CONDITIONAL MICROINJECTOR

3.1. Background and Preliminary Studies

Any of the previously mentioned pneumatic motors could be adapted to work with a linear guide and precision lead screw. However, the Geneva drive on this pneumatic motor allows for more accurate stepping and injection. In the context of linear travel, Tavallaei *et al.* developed a linear motion stage made suitable for the MR environment. Their device uses an ultrasonic motor (USM) and lead screw to accurately position a stage along a single axis within an MRI scanner. However, the accuracy is limited by the rotational speed of the USM; the positional error increases as the speed is increased [30]. Nofiele *et al.* developed a linear stage using two piezoceramic motors connected to linear bearings. Positional information was retrieved with an optical encoder. Their research was focused on acquiring accurate MRI images of a human abdomen by managing motion caused by respiration of a patient. The result was a platform that is much larger than one needed for syringe manipulation. Nevertheless, the system performed well within the designated displacement, velocity, and acceleration criteria for managing motion [31]. A major drawback of the devices created by Tavallaei *el al.* and Nofiele *et al.* is the price of the motors; both ultrasonic and piezoceramic motors can cost upwards of $1000. The devices used by by Tavallaei *el al.* and Nofiele *et al.* are shown in Figure 3.1.

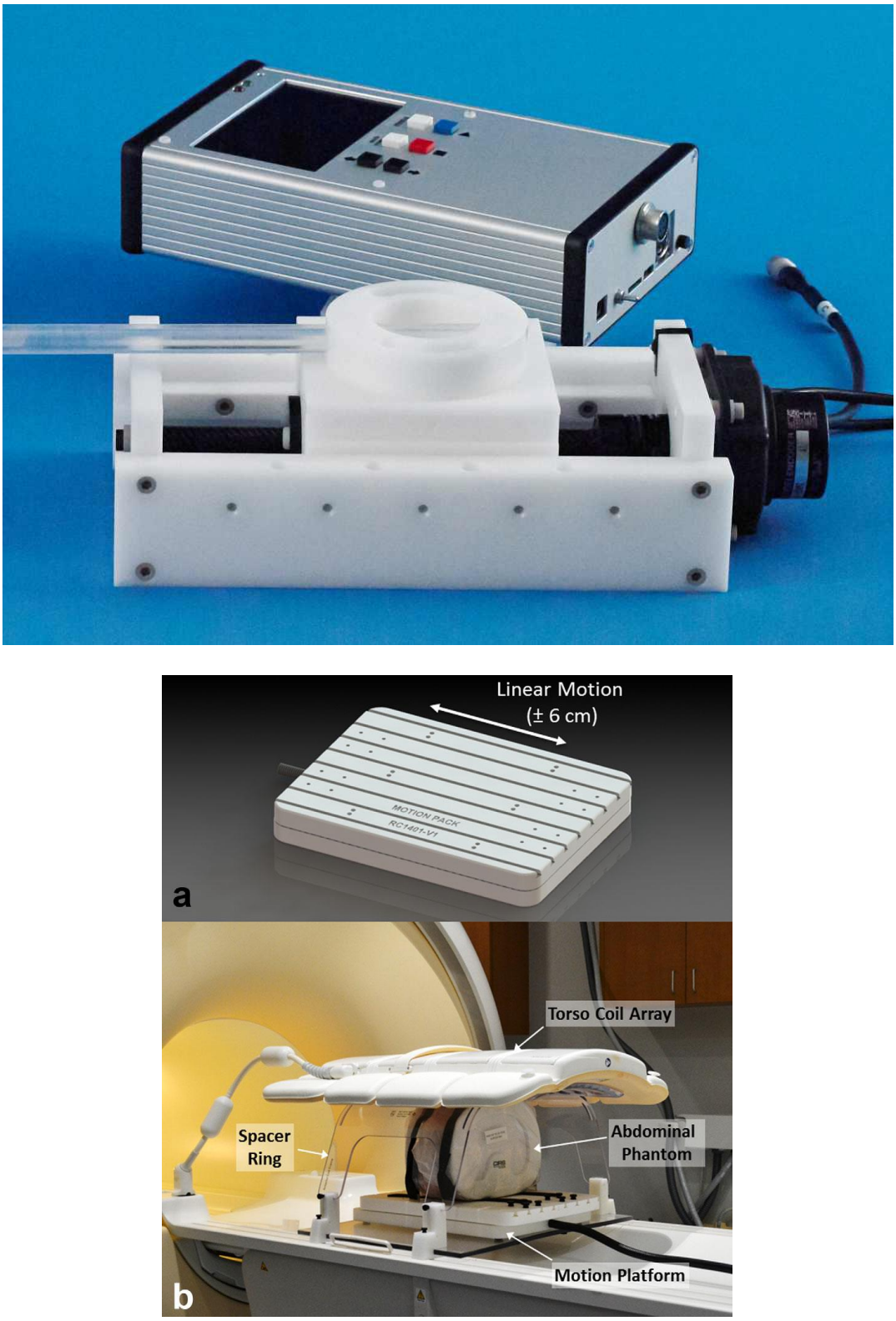

Figure 3.1: Linear motion stages by Tavallaei *et al.* (top) [32] and Nofiele *et al.* (bottom) [31]

Instead of positioning an object within an MRI machine, syringe pumps sit outside the scanner and inject liquid into a specimen. A linear motion stage could be converted to a syringe pump in theory, but syringe pumps are designed specifically to hold a variety of different size syringes and inject a precise amount of liquid into a test subject. Harvard Apparatus (Holliston, MA) and Chemyx (Stafford, TX) each offer an MRI Compatible syringe pump shown in Figure 3.2. However, both pumps contain some ferromagnetic components. Harvard Apparatus' pump must be placed at least five feet from the bore of the MRI scanner. More specifically, the pump must be placed where the actual field strength is less than 0.1 Tesla (1000 Gauss) [33]. In some cases, the syringe pump must be secured to a non-ferrous table or platform. Likewise, Chemyx's pump must be attached to a frame or platform while within the 0.05 Tesla (500 Gauss) line. Compared to the microinjector described in this thesis, the longer tubing of the Harvard Apparatus and Chemyx syringe pumps can cause less accurate and less consistent results. Again, a major drawback of these systems is cost. Harvard Apparatus' syringe pump is priced at over $5000, and the system made by Chemyx costs $1600.

Figure 3.2: The Harvard Apparatus BS4 70-2130 (top) is an MRI Compatible syringe pump, but it must be placed at least five feet from the bore of the MRI scanner [33]. The Chemyx NanoJet MRI Syringe Pump (bottom) can be used within the 0.05 Tesla (500 Gauss) line but must be secured to a frame [34].

3.2. Assembly of Microinjector

The injector is made entirely of nonferrous and nonmagnetic materials so that it is compatible with the MR environment. The pneumatic stepper motor is attached to one end of a linear guide (Part Number: SWX-104001, igus, East Providence, RI, USA). A syringe is attached to the other end of the linear guide using customized adaptors. At the end of the syringe is an apparatus for filling the tubing with water. The apparatus is also used for removing air bubbles from the system and equalizing the pressure in the tubing after the set up process. Figure 3.3 shows the device in its current configuration.

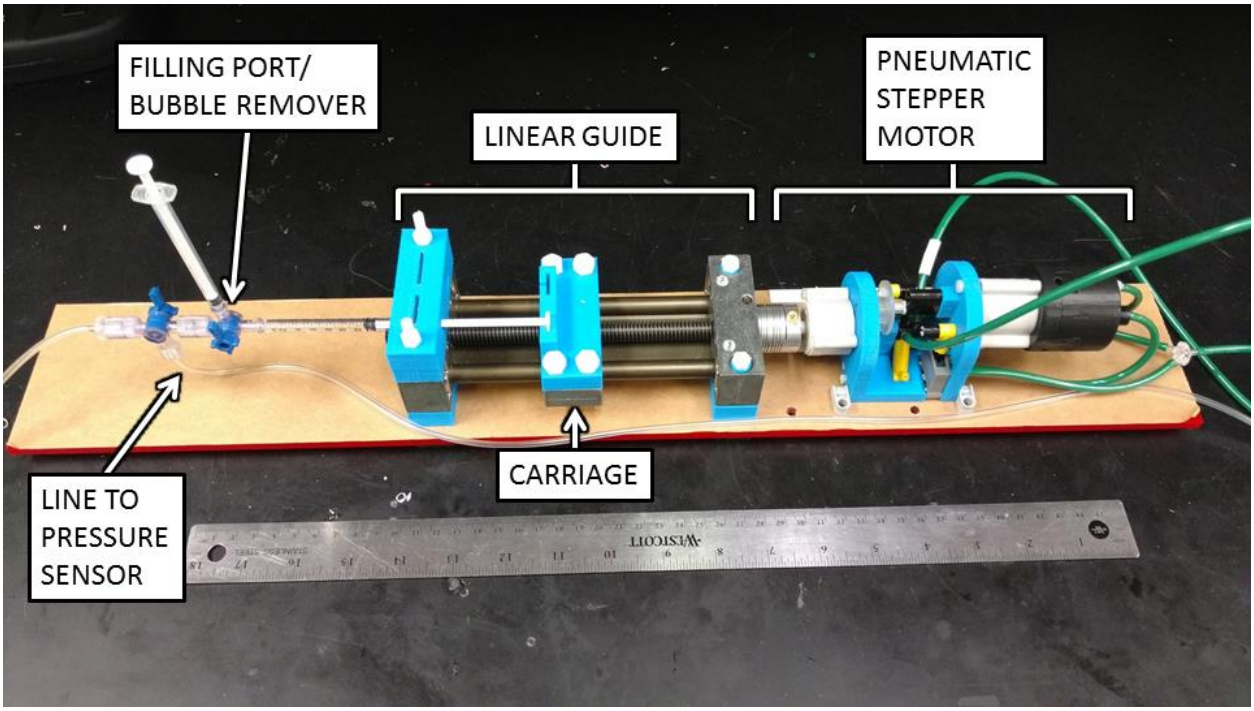

Figure 3.3: Above is a prototype of the presented microinjector. To the far left is the filling apparatus and line to pressure sensor. The linear guide with syringe holder is in the center. The pneumatic motor is to the right. Currently, the smallest size of syringe is attached.

3.3. Control Electronics and Software

Figure 3.4 shows the interior view of the control electronics. As mentioned in Chapter 2, the system uses a DAQ card, two 3-way pneumatic solenoid valves, a valve driver circuit to power the valves, and an air supply source. The only additional hardware is a gauge pressure sensor (SSCDANT005PGAA5, Honeywell, Golden Valley, MN, USA). A wiring diagram can be found in Appendix A at the end of the thesis.

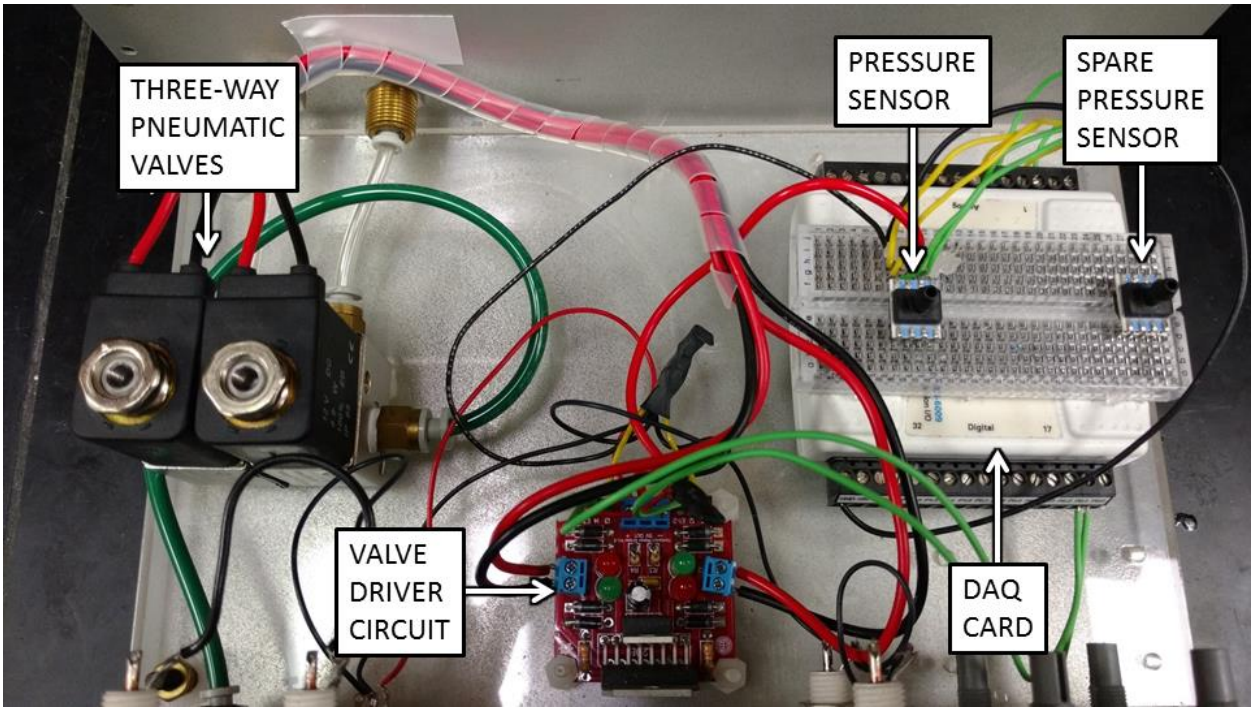

Figure 3.4: Above is the interior view of the control box. To the left are two 3-way valves to operate the pneumatic cylinders. The DAQ card is at the right along with the pressure sensor. The circuit board that drives the valves is at the bottom.

The front panel of the software is shown in Figure 3.5. The control software for the stepper motor is integrated into the software for the microinjector. Before pressing the run button, the user must set the file paths for the initialization file and data logging file. The initialization file stores parameters for the syringe size last used and the last known displacement

of the carriage. The data log file stores parameters such as pressure, volume, displacement, system messages, and time. The program is written for three syringe sizes so that plunger travel length and volume displaced are properly calculated. The applied pressure, volume displaced, and carriage displacement are constantly monitored. Applied pressure is displayed by a dial gauge and a waveform chart. Control operations include Auto Seek Pressure, Auto Seek Volume, Inject One Step, Retract One Step, and Fully Retract. An option to maintain desired pressure is available while using the Auto Seek Pressure control mode. If Maintain Pressure is turned on and the pressure drops below the threshold, the pump will activate until desired pressure is once again achieved. System messages and errors are displayed at the bottom of the interface. The main functions of the program are illustrated and detailed in Appendix B.

During clinical trials, the operator is able to set a desired applied pressure or set a desired volume to be injected. The operations are automatic; however, manual control of the injector is also available. If using the Auto Seek Pressure feature to find a pressure greater than the current pressure, the stepper motor advances the plunger of the syringe until the desired pressure is attained. Then the device resorts to standby if Maintain Pressure is not activated. If seeking a pressure less than the current pressure, the motor retracts the plunger until pressure is below the threshold. Then the motor reverses direction and injects until the pressure is greater than or equal to the desired level before resorting to standby. Figure 3.6 shows a flowchart of the Auto Seek Pressure process.

While using Auto Seek Volume, the program resorts to standby after the desired volume has been displaced. Auto Seek Volume works for injection only. The number of steps is monitored by the software so that if the carriage of the linear guide has reached its physical

limits, the system resorts to standby and an error message is displayed. Figure 3.7 shows a flowchart of the Auto Seek Volume process.

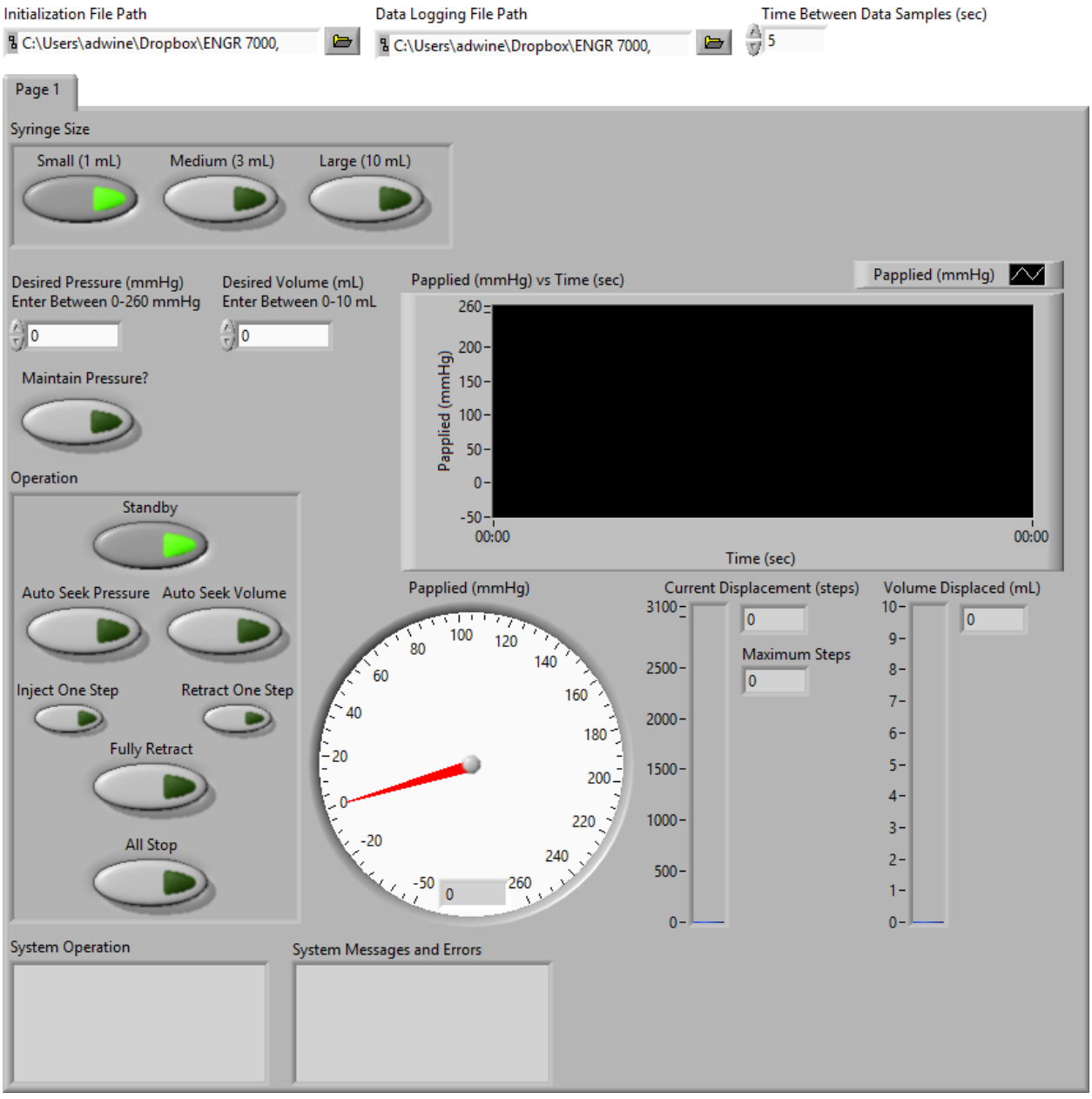

Figure 3.5: The front panel of the LabVIEW microinjector software

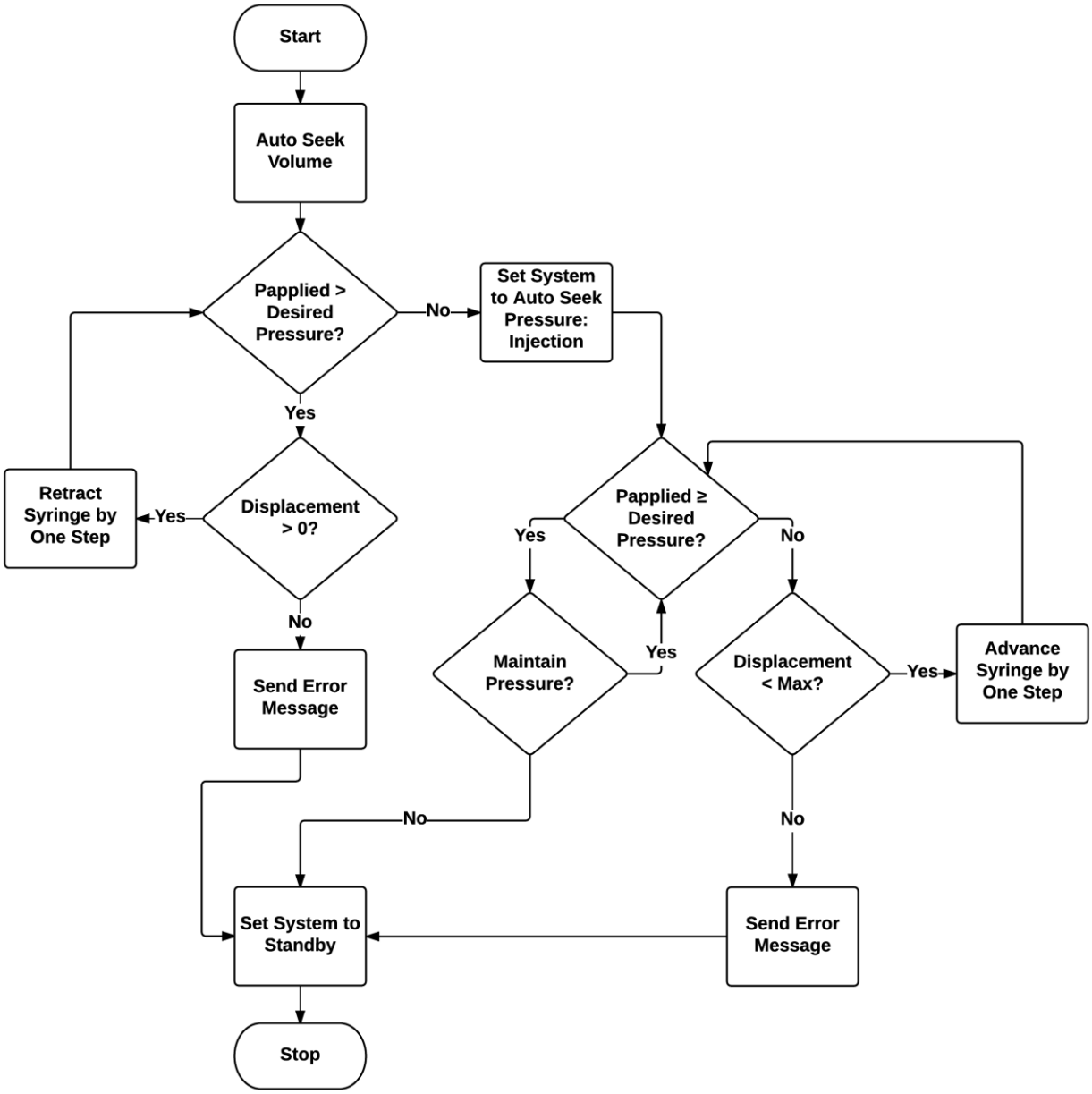

Figure 3.6: A flowchart of the Auto Seek Pressure control mode

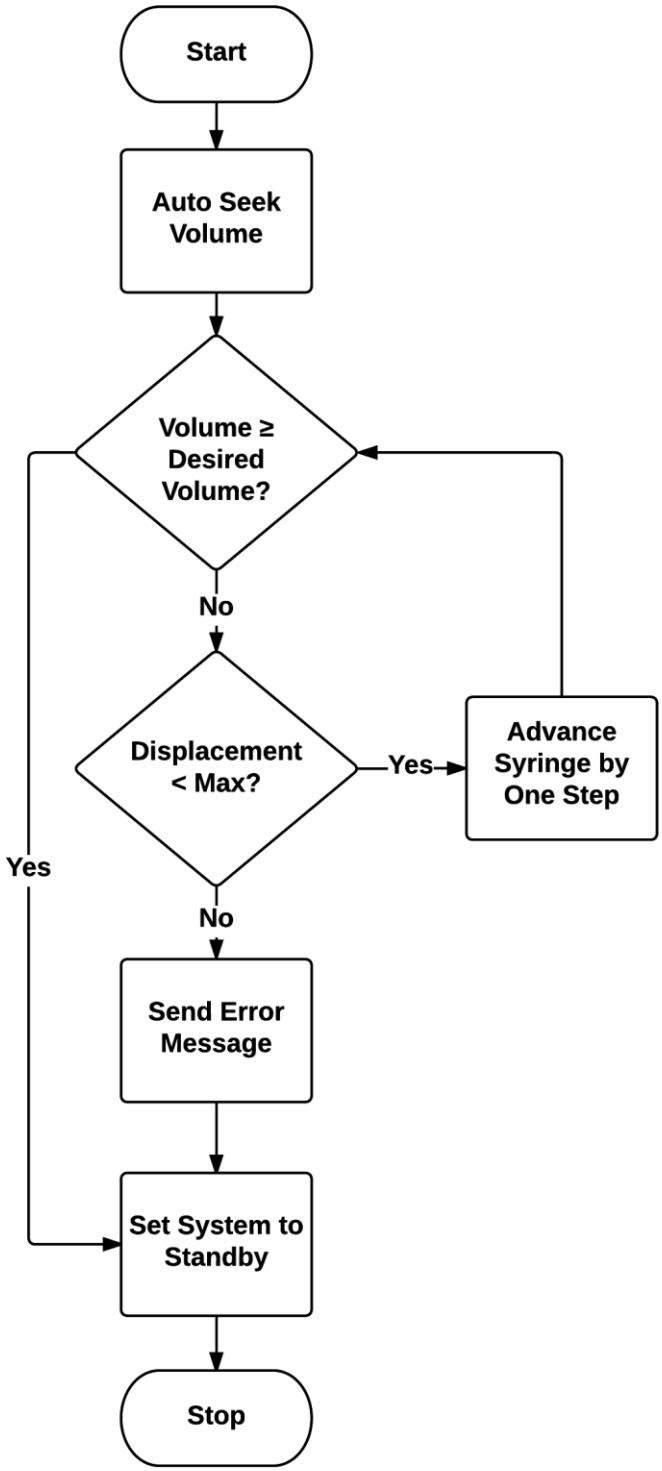

Figure 3.7: A flowchart of the Auto Seek Volume control mode

3.4. Working Principle

The pneumatic stepper motor rotates the lead screw causing the carriage to shift forward or backward. For each full rotation of the lead screw, the carriage will advance 2 mm. Since the stepper motor advances 3.6 degrees per step, the carriage moves 0.02 mm per step. The volume of fluid injected depends on the size of the syringe. The injector was designed to hold three different sizes of syringes (Nipro Medical Corporation, Bridgewater, NJ, USA). The largest syringe for the microinjector holds 10 mL per 61 mm, or approximately 0.164 mL/mm. Therefore, for each step of the motor, the liquid inside the syringe is displaced by about 0.00328 mL, or 3.28 µL. The medium-size syringe holds 3 mL per 42 mm, which is approximately 0.0714 mL/mm. For each step, the liquid is displaced by approximately 1.43 µL. The smallest syringe holds 1 mL per 57.25 mm, or approximately 0.0175 mL/mm. Therefore, liquid is displaced by approximately 0.349 µL per step. Table 3.1 compares parameters of the three different syringe sizes.

	Syringe Size		
	Large	Medium	Small
Plunger Travel Length	61 mm	42 mm	57.25 mm
Plunger Travel Length in Steps	3050 steps	2100 steps	2862.5 steps (2862 steps)
Volume (mL) per mm	0.164 mL/mm	0.0714 mL/mm	0.0175 mL/mm
Volume (µL) per Step	3.28 µL (0.00328 mL)	1.43 µL (0.00143 mL)	0.349 µL (0.000349 mL)

Table 3.1: Parameters of three different syringe sizes

3.5. Experimental Setup

Testing the efficacy of the microinjector involved inserting a non-magnetic catheter needle (NIC-20GX2", Nipro Medical Corporation, Bridgewater, NJ, USA) into a series of sheep eyeballs (Carolina Biological Supply Company, Burlington, NC, USA) and injecting water into an eyeball in order to inflate and stretch the sclera. Initial tests involved capturing images of an eyeball using an 8 megapixel camera set to a time-lapse mode. MRI was later used to view an eyeball's interior anatomical structure. For experiments utilizing the camera, the pressure was logged every five seconds, and images were captured every thirty seconds.

For MRI trials, the computer was located in the control room along with the control box which contains the DAQ card, valves, valve driver circuit, and pressure sensor. The microinjector is located in front of the bore of the MRI scanner. The pressurized air is supplied by an air compressor. Figure 3.8 illustrates the typical layout of a clinical setup.

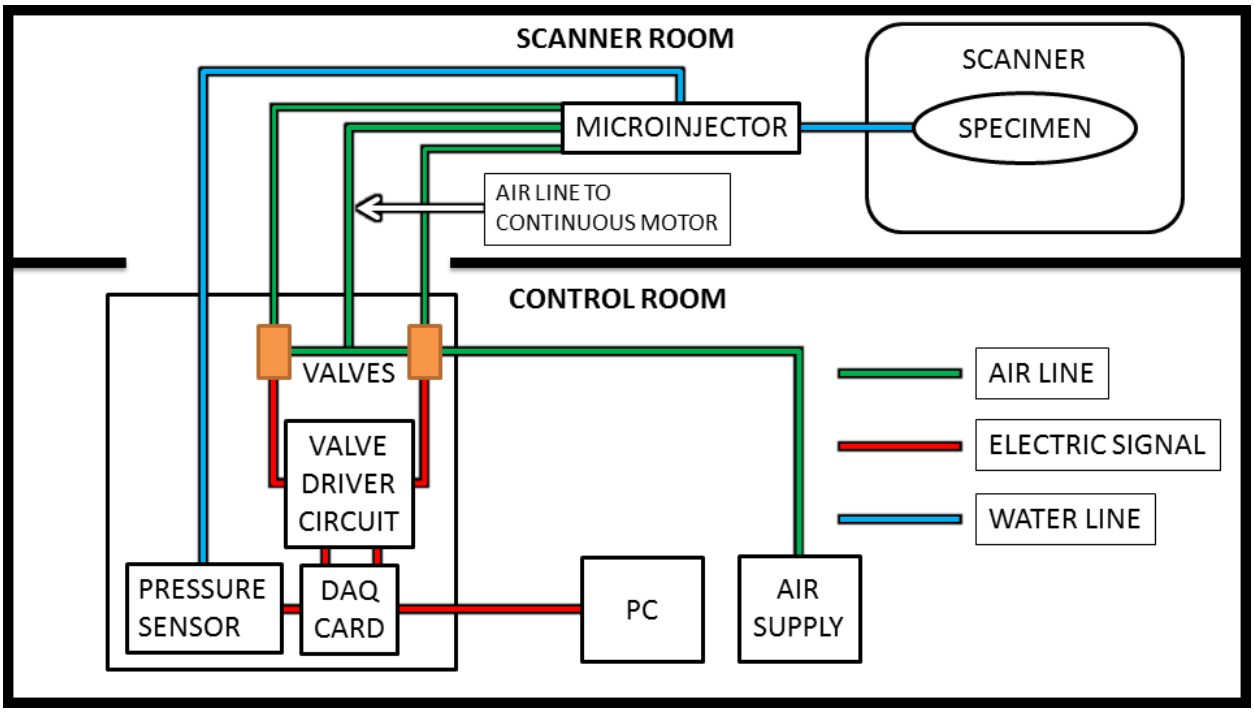

Figure 3.8: During clinical trials, the microinjector is near the bore of the MRI scanner. A line from the output of the microinjector travels back to the pressure sensor inside the control box. The control box, PC, and air compressor are in the control room.

3.6. Test Results

Figures 3.9a and 3.9b are images taken from one of the experiments using the 8 megapixel camera. Although some changes in the eyeball's structure are obvious, subtle changes in size were highlighted by taking the absolute difference of the images using MATLAB (Figures 3.9c). The complement of the absolute difference is given for visual clarity (Figure 3.9d). Figure 3.10 is a montage of the eyeball at different pressures (0 mmHg, 20 mmHg, 40 mmHg, 60 mmHg, 80 mmHg, and 100 mmHg). Table 3.2 compares the pressure and volume injected in 20 mmHg intervals.

MRI images were taken with a Varian Magnex 7 Tesla MRI system using the fast spin-echo (FSE) sequence. Scans were taken every 20 mmHg starting at 0 mmHg and ending at 100 mmHg. Each scan slice is 4 mm thick. Figures 3.11a and 3.11b show the images acquired during MRI tests. Figure 3.11a is a montage of the eyeball at 0 mmHg. Figure 3.11b contains images taken with the eyeball inflated to 100 mmHg. Using MATLAB, the absolute difference of Figures 3.11a and 3.11b was taken to highlight subtle changes in size and structure (Figure 3.11c). Again, the complement of the absolute difference is given for visual clarity (Figure 3.11d). Figure 3.12 is a montage of the sixth slice from each pressure setting (0 mmHg, 20 mmHg, 40 mmHg, 60 mmHg, 80 mmHg, 100 mmHg). This slice was chosen because it is closest to the center of the eyeball. Change in shape of the eyeball is obvious in the lower right corner of each subsequent image. Volume and pressure for MRI trials are compared in Table 3.3. The volume of liquid injected at 100 mmHg during MRI trials is 0.35 mL more than trials with the camera. This is most likely due to a leak in the system or the eyeball. And since MRI scans take considerably longer than pictures, a leak allowed more water to escape.

Figure 3.9a: Above is a raw image at t = 0 sec, pressure = 0 mmHg, and volume injected = 0 mL. The needle can be seen on the left.

Figure 3.9b: Above is a raw image at t = 535 sec (8 min 55 sec), pressure = 100 mmHg, volume injected = 1.75 mL. The needle can be seen on the left.

Figure 3.9c: The absolute difference of the images in Figures 3.9a and 3.9b creates light areas which indicate differences between the images. The light line surrounding the eye indicates that the eye inflated in all directions.

Figure 3.9d: The complement of absolute difference in Figure 3.9c creates dark areas which indicate differences between the images. The dark line surrounding the eye indicates that the eye inflated in all directions.

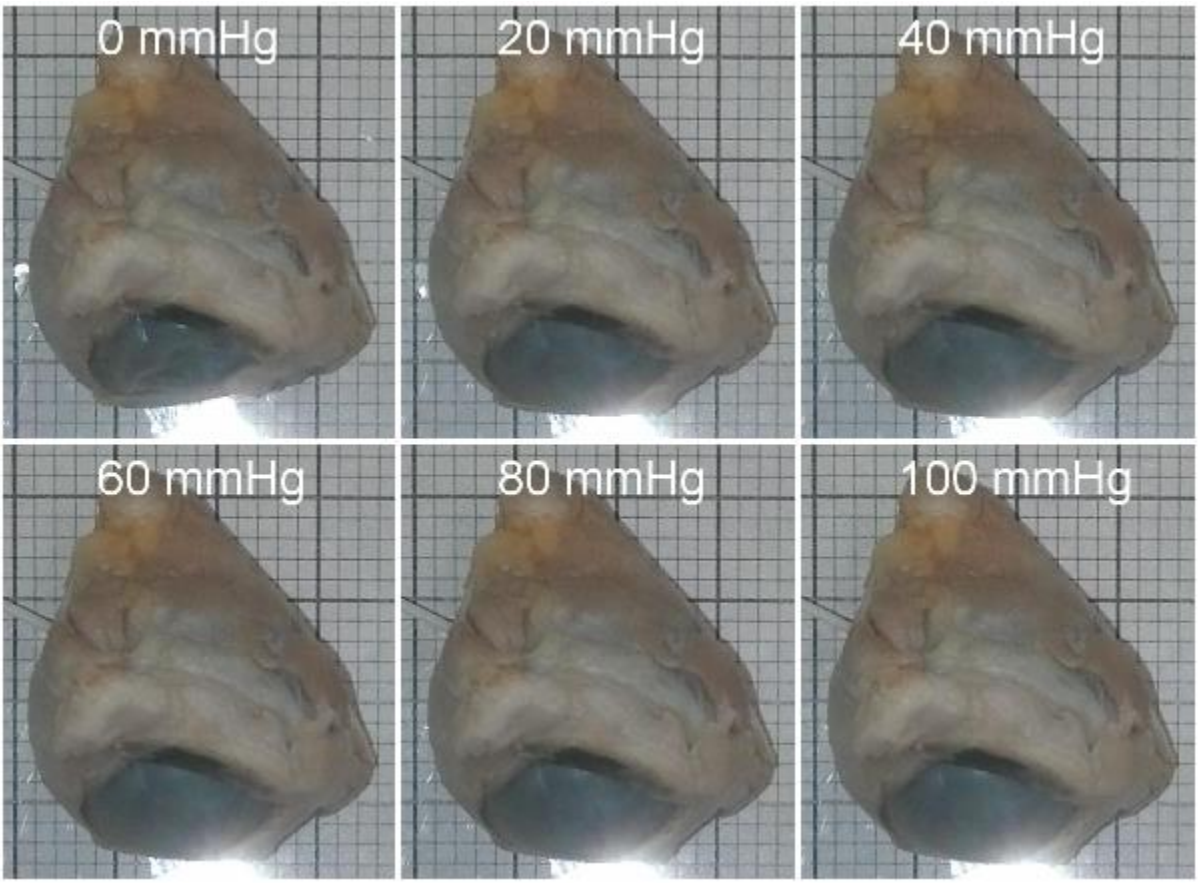

Figure 3.10: A montage of the eyeball at discrete pressures

Approximate Pressure	0 mmHg	20 mmHg	40 mmHg	60 mmHg	80 mmHg	100 mmHg
Volume Injected	0 mL	.85 mL	1.11 mL	1.36 mL	1.56 mL	1.75 mL

Table 3.2: A comparison of the pressure and volume injected during trials with the 8 megapixel camera

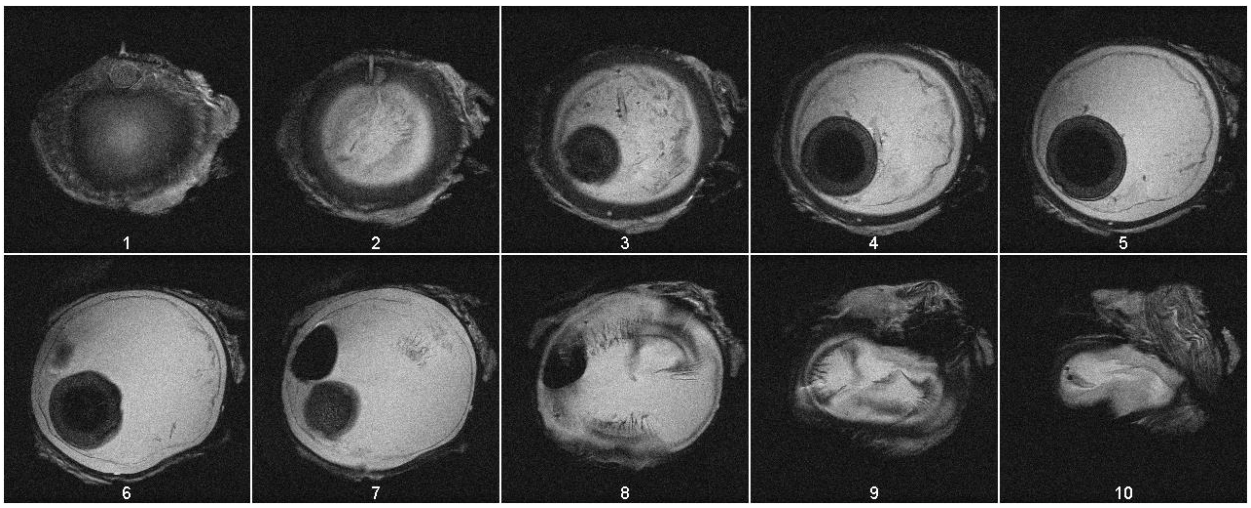

Figure 3.11a: Above is a montage of the eyeball at 0 mmHg. The first image slice is the bottom of the eyeball, and the last image slice is the top of the eyeball. Each image slice is about 4 mm thick. The opening of the bore is toward the top of each image.

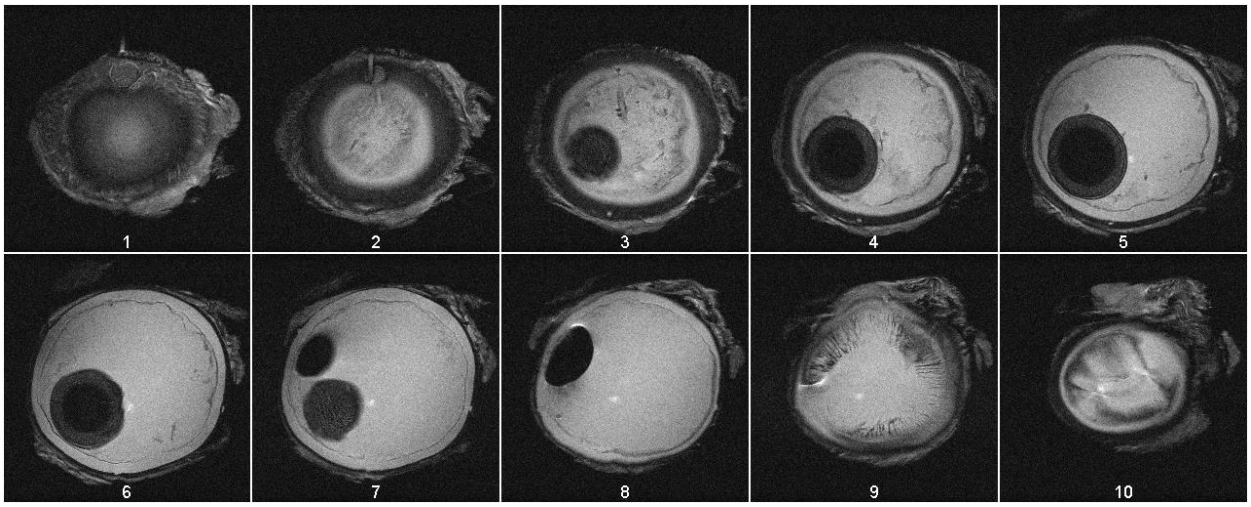

Figure 3.11b: Above is a montage of the eyeball at approximately 100 mmHg injected with 2.1 mL of water. The first image slice is the bottom of the eyeball, and the last image slice is the top of the eyeball. Each image slice is about 4 mm thick. The opening of the bore is toward the top of each image.

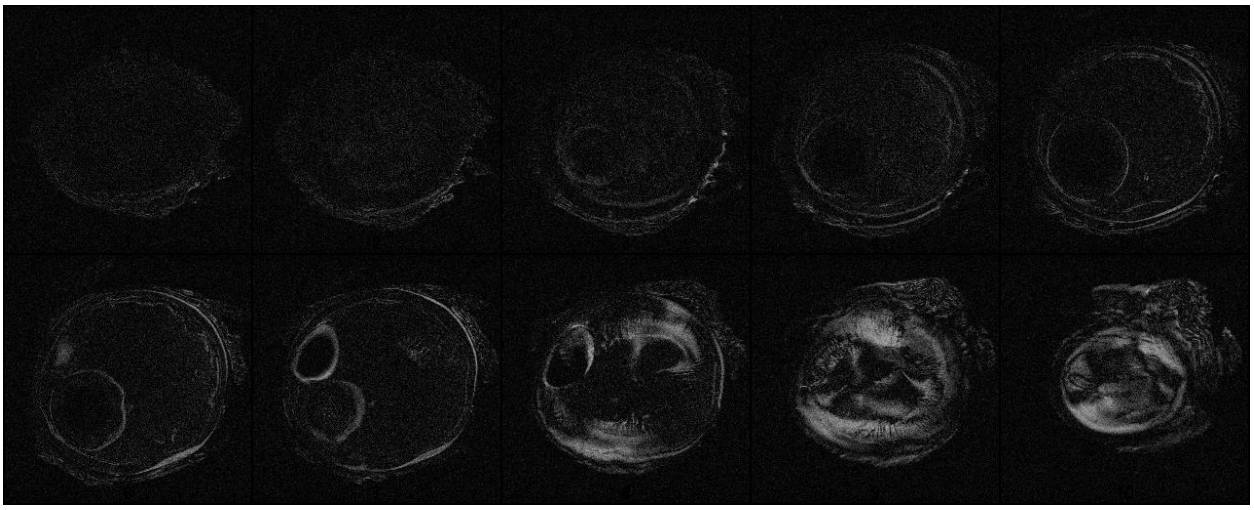

Figure 3.11c: The absolute difference of the montages in Figures 3.11a and 3.11b creates light regions which indicate differences in the two compared images.

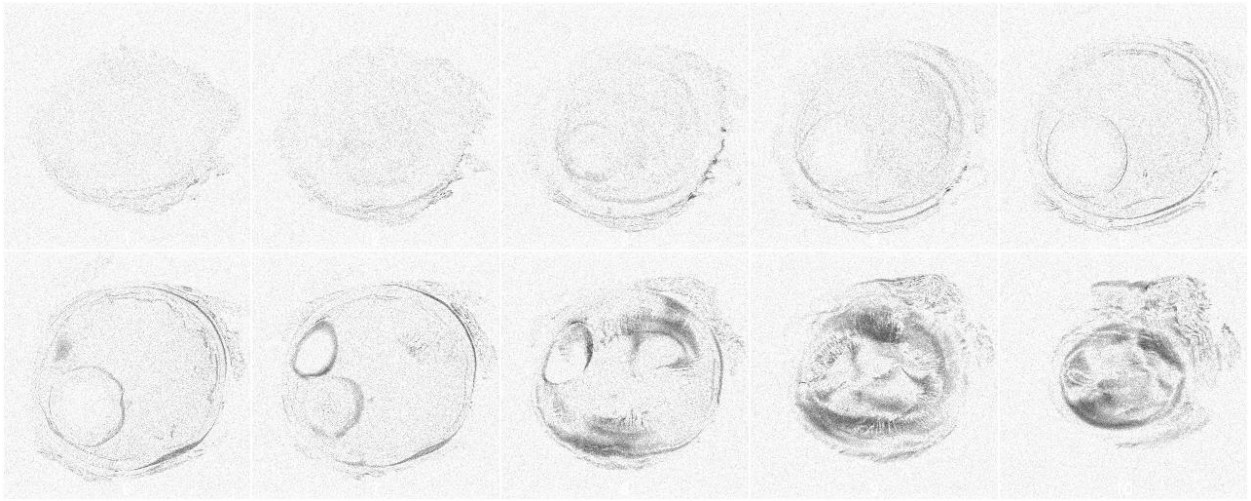

Figure 3.11d: The complement of the absolute difference creates dark regions which indicate differences in the two compared images.

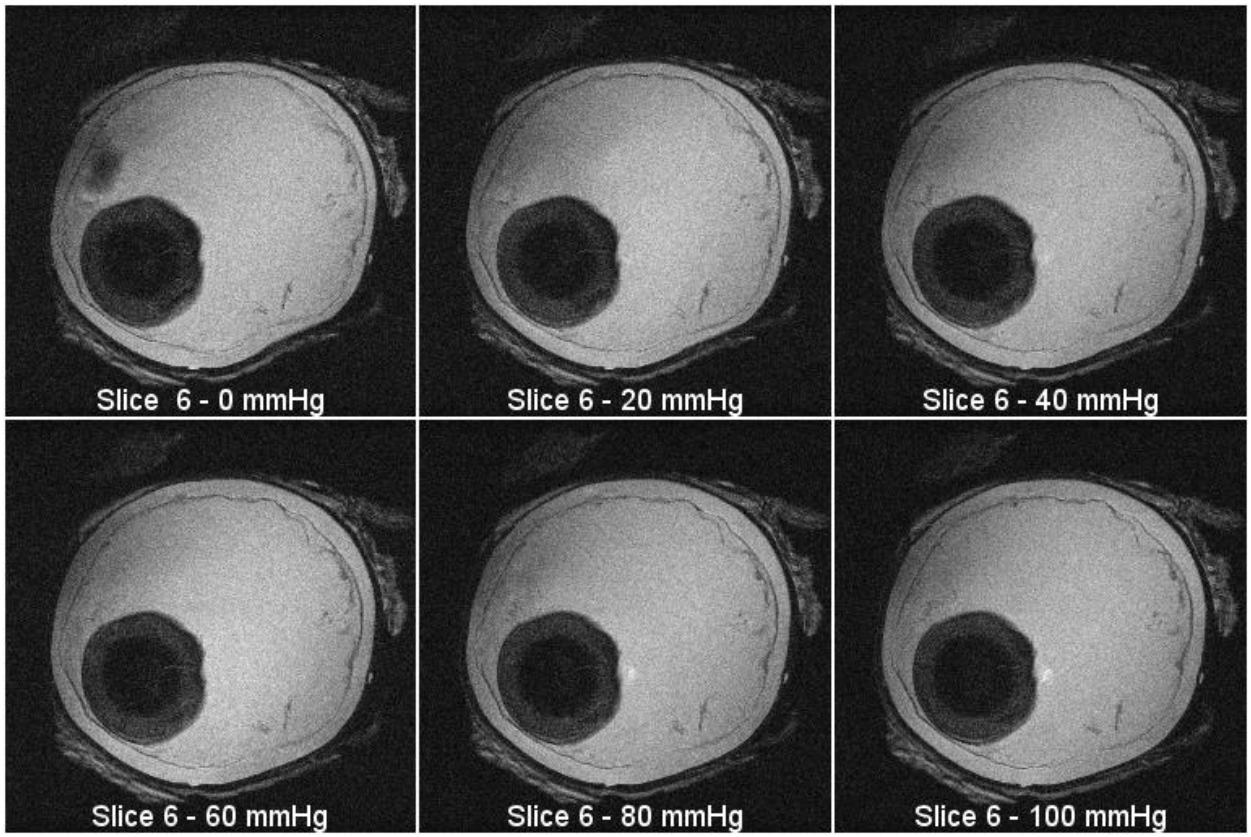

Figure 3.12: MRI Slice 6 from each pressure setting

Approximate Pressure	0 mmHg	20 mmHg	40 mmHg	60 mmHg	80 mmHg	100 mmHg
Volume Injected	0 mL	.8 mL	1.2 mL	1.55 mL	1.85 mL	2.1 mL

Table 3.3: A comparison of the pressure and volume injected during MRI trials

3.7. MRI Safety Information

The term *MR compatible* has been replaced with *MR Conditional*. Previously, *MR safe* and *MR compatible* were defined as follows [19]:

> *MR safe* — This term indicates that the device, when used in the MR environment, has been demonstrated to present no additional risk to the patient but may affect the quality of the diagnostic information.
>
> *MR compatible* — This term indicates that the device, when used in the MR environment, is MR safe and has been demonstrated to neither significantly affect the quality of the diagnostic information nor have its operations affected by the MR device.

The terminology was sometimes used incorrectly or interchangeably. Therefore, a new set of terms was developed by the American Society for Testing and Materials (ASTM) International. According to the most recent ASTM F2503 standard, the definitions for MR Safe, MR Conditional, and MR Unsafe are as follows [35]:

> *MR Safe* — an item that poses no known hazards resulting from exposure to any MR environment. MR Safe items are composed of materials that are electrically nonconductive, nonmetallic, and nonmagnetic.
>
> *MR Conditional* — an item with demonstrated safety in the MR environment within defined conditions. At a minimum, address the conditions of the static magnetic field, the switched gradient magnetic field and the radiofrequency fields. Additional conditions, including specific configurations of the item, may be required.
>
> *MR Unsafe* — an item which poses unacceptable risks to the patient, medical staff or other persons within the MR environment.

The signal to noise ratio (SNR) generated by the microinjector was tested under three conditions using the spin-echo (SE) sequence of a Varian Magnex 7 Tesla MRI system. All three test conditions were conducted with a phantom placed inside the bore of the magnet. Each test was run for three slices of the phantom, resulting in nine images total. The baseline for the experiment was conducted with the device completely off. For the next scan, the electronics

were powered on, but the motor sat idle. The third scan was made with the motor in operation. Figures 3.13a and 3.13b compare the baseline image to the images of the motor idle and the motor in operation, respectively.

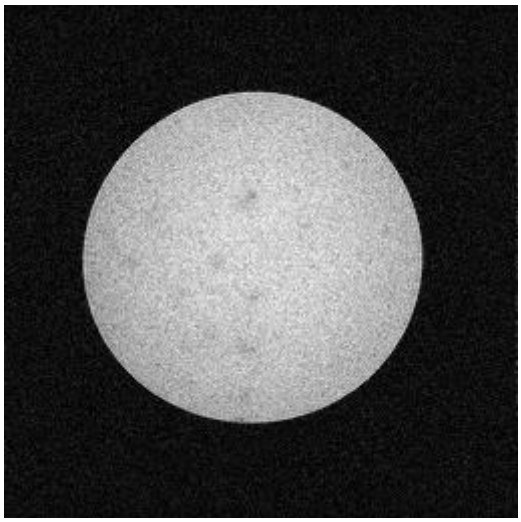

Baseline

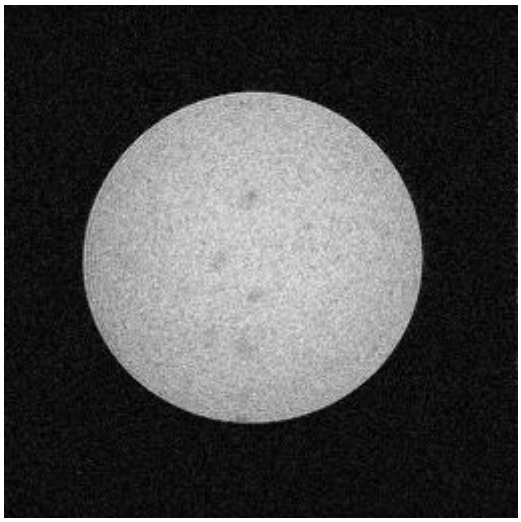

Motor Idle

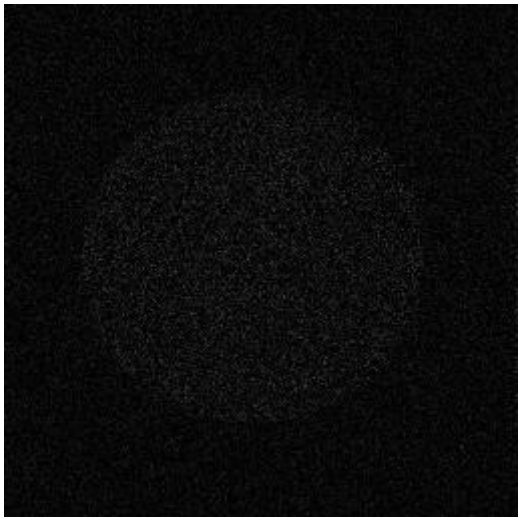

Absolute Difference

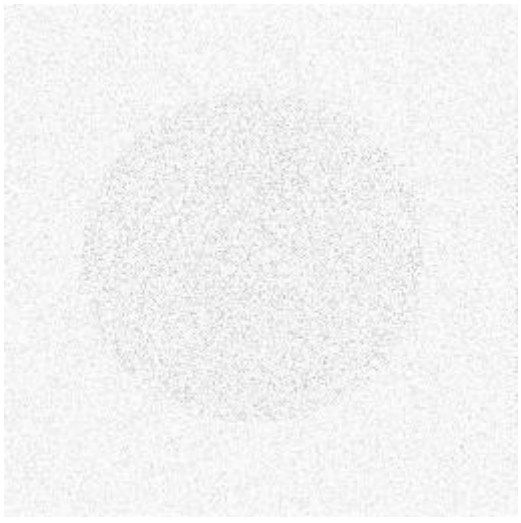

Complement

Figure 3.13a: Above is a comparison of the images acquired during the baseline condition and the motor idle. The baseline image is at the top left. The image of the phantom with the motor idle is at the top right. The bottom row shows the absolute difference of the top two images (left) and its complement (right).

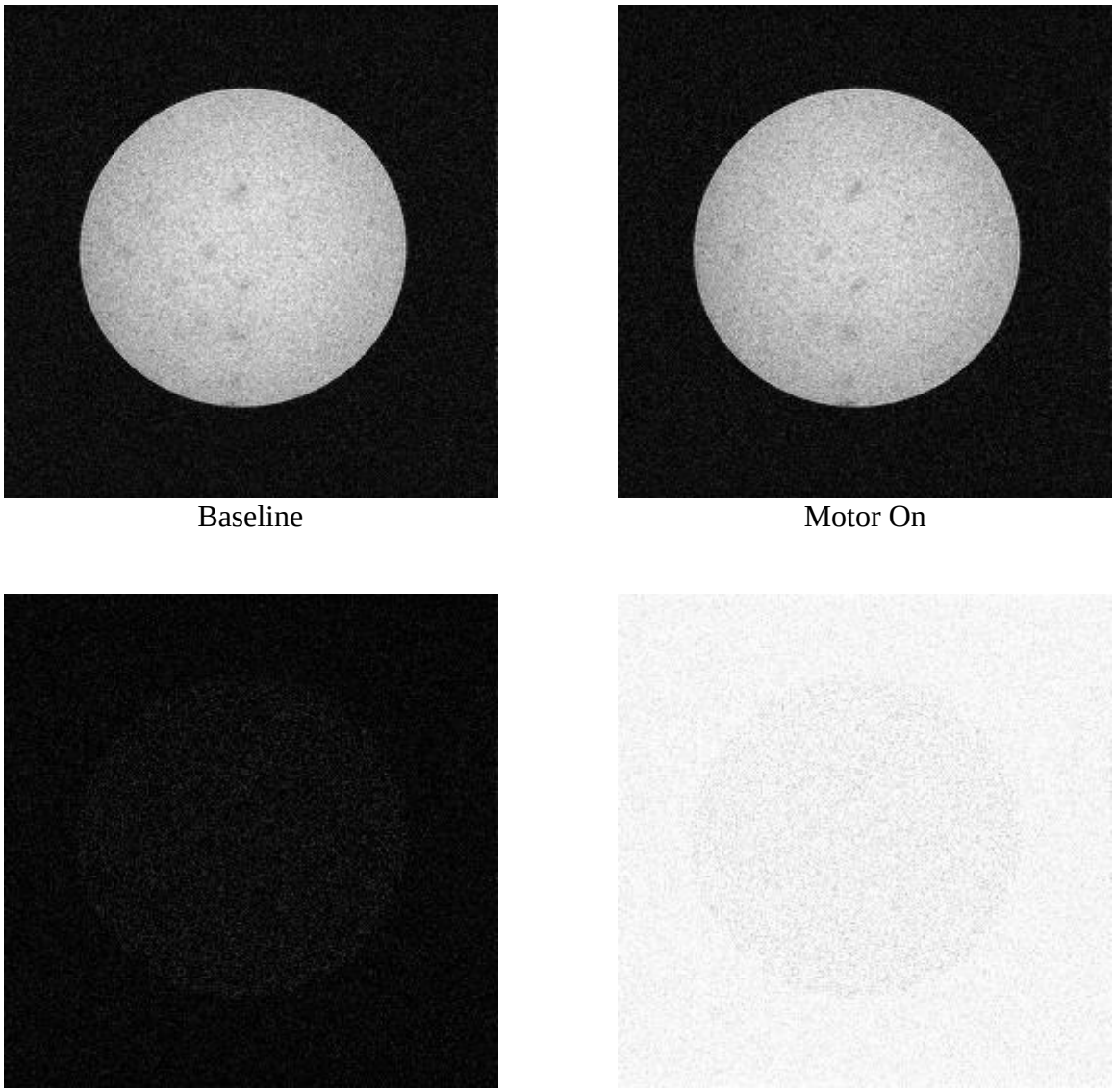

Figure 3.13b: Above is a comparison of the images acquired during the baseline condition and the motor in operation. The baseline image is at the top left. The image of the phantom with the motor on is at the top right. The bottom row shows the absolute difference of the top two images (left) and its complement (right).

The SNR was calculated with the following equation:

$$SNR = \frac{I_{center}}{SD_{corner}}$$

where I_{center} is the mean of pixel intensity at the center of an image slice and SD_{corner} is the standard deviation of the pixel intensity at the corner of an image slice. Values were measured using a 40 x 40 pixel square.

Figure 3.14 shows a comparison of the signal to noise ratios generated by each condition. Table 3.4 shows the comparison of SNR and reduction. On average, the baseline produced an SNR of around 25.9, converting to decibels yields $10\log_{10} 25.9 = 14.13\ dB$. With the system powered on and the motor idle, the SNR is approximately 24.9 (13.96 dB), a reduction of about 3.86%. When the motor is running, the SNR is approximately 25.6 (14.08 dB), resulting in a reduction of approximately 1.16%. It is expected that when the motor is running that a greater SNR should develop compared to when the motor is idle. Several checks were made to ensure the correct numbers and equations were used; surprisingly, the SNR of the Motor On condition is indeed greater than when the motor is idle. The difference, however, is negligible. What matters is that each condition have less than 10% reduction of the baseline SNR, which is the case [18].

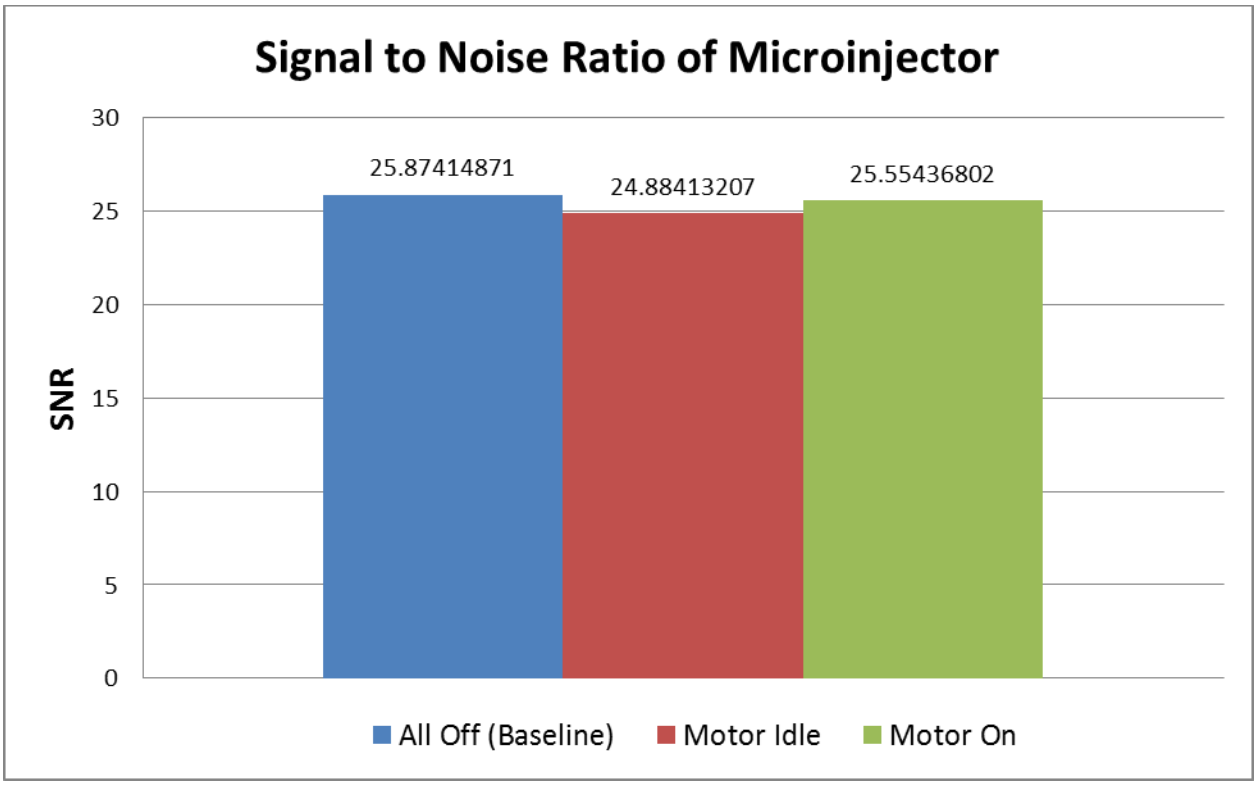

Figure 3.14: A comparison of SNR of the microinjector under three test conditions

	Baseline	Motor Idle	Motor On
SNR	25.9	24.9	25.6
SNR ($10\log_{10} SNR = SNR\ dB$)	14.13 dB	13.96 dB	14.08 dB
Percent Reduction	0%	3.86%	1.16%

Table 3.4: A comparison of the SNR reduction using the spin-echo sequence

CHAPTER 4:

CONCLUSIONS AND FUTURE WORK

4.1. Summary of Work

This thesis discussed the development and evaluation of an MR Conditional stepper motor and microinjector. Chapter 1 introduced the background to glaucoma, microinjection, and magnetic resonance imaging. Chapter 2 detailed the design and development of a pneumatic stepper motor capable of operation within an MR environment. Chapter 3 applied the pneumatic stepper motor to a linear guide to create a microinjection system also capable of operation within a field of high magnetic resonance. The microinjection device was developed primarily as an inflation test system to study intraocular pressure and its connection to glaucoma. MRI was chosen as the principle means to acquire images because it is able to view subtle changes in the anatomical structure of the eyeball without having to excise any tissue. Therefore, the microinjector was developed to be compatible with high magnetic resonance; traditional components with ferromagnetic materials pose a hazard as well as affect image quality. The efficacy of the microinjector was tested by inflating sheep eyeballs in vitro and imaging the eyeballs with a 7 T MRI scanner. The microinjector successfully inflated the eyes without causing any artifacts in the images, and the magnetic field of the scanner did not affect the performance of the microinjector. The microinjector is considered MR Conditional because its compatibility has only been tested in a 7 T environment. Although it is reasonable to assume similar performance in other field strengths, there still exists a possibility that the microinjector behaves differently or affects image quality.

4.2. Future Work

Despite a successful development, several modifications and optimizations are being considered. For instance, the chassis of the stepper motor can be made smaller by using a single 3-way pneumatic switch instead of the two that are installed. As it is now, only two ports of each switch are being utilized, which unnecessarily increases the overall physical dimensions. The reason for having two 3-way switches is due to the physical limitations of the switch-cylinder combination; there was not a noticeable way to connect two Lego cylinders to one Lego switch. Custom cylinders need to be developed in order to use a single 3-way Lego switch. Another alternative configuration of the chassis components involves using two 2-way switches. In which case the switches would need to be custom-designed, and the Lego cylinders could still be utilized.

The resistance of the pneumatic switches to change position requires the continuous motor to output a substantial amount of torque, reducing the desired trait of speed. One way to reduce the demand for torque is to minimize the amount of friction inside the switches by making custom switches. In addition, the cam could be outfitted with a bearing on the end that makes contact with the switches. That way, the cam would not have to rub against the switch and cause excessive friction.

The range of operating pressures for the stepper motor is small. A precise amount of pressure and air flow is required to achieve optimal performance. Faster stepping speeds are possible with higher pressures, but the steps are uncountable. In other words, a single pulse at high pressure might cause the main axle (the Geneva pinned gear and cam) to rotate twice because of excessive inertia. The inertia needs to be controlled, and the cam needs to be stopped

at vertical after each signal. To accomplish this, a detent or braking system could be implemented.

The Geneva drive was fabricated using additive manufacturing technology, commonly known as 3D printing. The product made by the printer required some finishing and post-processing work in order to compensate for imperfect dimensions. Since a proof-of-concept has been established, future Geneva drives will be made from a stronger material and with tighter tolerances. Accuracy is likely to improve, albeit slightly, since the pin will better fit the slots, and the stop disc will be more snug. Stronger material will render the pin less susceptible to separation from its gear. It would also be interesting to compare performance of the stepper motor using additional slots in the slotted gear, an internal Geneva drive, or a different indexing mechanism altogether.

Regarding improvements to the microinjector, the first modification would be adding a quick-release button to the carriage only because installing a syringe has proven to be most frustrating and time-consuming. The carriage has to be at the exact location of the plunger's end in order to install a syringe. A quick-release button would allow the carriage to detach from the lead screw and be rapidly positioned at the correct location, saving valuable time.

The linear guide assembly is metal. While it is nonmagnetic and poses virtually no threat to patients, personnel, or images, the metal needs to be replaced. The metal frame adds needless bulk and weight to the overall design. Creating a linear guide out of lightweight, MR Safe material would allow the microinjector to fit in smaller spaces or be placed on a stereotactic frame.

While operating the microinjector, the only way to know when the carriage has reached the end of the lead screw is by counting the number of steps. A better approach would be to

implement a sensor or button to the ends of the linear guide to prevent the device from damage. Perhaps an optical sensor could relay a stop command back to the control box. Another idea is to install a momentary pneumatic switch at each end of the guide to prevent airflow to the motor. One switch corresponds to clockwise, and the other is for counterclockwise. When the carriage reaches a maximum, it pushes the switch open allowing air to escape. The motor is then operated in the opposite direction causing the switch to close. This approach would prevent damage, but there would not be any feedback to alert the operator that the carriage is at a maximum.

After a few optimizations, future work would involve using the microinjector for procedures other than inflation testing. The microinjector combined with MRI could prove useful in delivering drugs and therapeutics to small targets in otherwise hard to see places. The microinjector could be used in conjunction with other robotic systems to aid in image-guided surgeries.

4.3. Thesis Contributions

The microinjector presented in this thesis will help researchers study intraocular pressure and its correlation to glaucoma. Together with MRI, researches will be able to view changes and deformations of the tissue inside an eyeball at designated pressures. Compared to the few commercially available MR-compatible syringe pumps and linear motion stages, this microinjector offers a solution at a much lower price. The total system costs less than $700. In addition, the presented microinjector is capable of being placed next to the bore of the scanner enabling researchers to perform MRI-guided procedures that require precise pressure and volume manipulations.

The stepper motor powering the microinjector offers a unique approach to the limited number of MR Conditional stepper motor designs. It offers an alternative to actuators that require complex, expensive sensors and encoders. And with the field of MRI-guided robotic surgery expanding rapidly, researchers are in need of new perspectives to further develop precise and efficient instruments.

REFERENCES

[1] Glaucoma.org. (2010, October 25). *Types of Glaucoma*. Available: http://www.glaucoma.org/glaucoma/types-of-glaucoma.php

[2] M. A. Fazio, R. Grytz, L. Bruno, M. J. Girard, S. Gardiner, C. A. Girkin, *et al.*, "Regional variations in mechanical strain in the posterior human sclera," *Investigative ophthalmology & visual science*, vol. 53, p. 5326, 2012.

[3] T. D. Nguyen and C. R. Ethier, "Biomechanical assessment in models of glaucomatous optic neuropathy," *Experimental eye research*, vol. 141, pp. 125-138, 2015.

[4] L. C. Ho, I. A. Sigal, N.-J. Jan, A. Squires, Z. Tse, E. X. Wu, *et al.*, "Magic Angle–Enhanced MRI of Fibrous Microstructures in Sclera and Cornea With and Without Intraocular Pressure LoadingMRI of Fibrous Microstructures in the Eye," *Investigative ophthalmology & visual science*, vol. 55, pp. 5662-5672, 2014.

[5] J. C. Tsai. (2015, October 25). *High Eye Pressure and Glaucoma*. Available: http://www.glaucoma.org/gleams/high-eye-pressure-and-glaucoma.php

[6] A. Elsheikh, D. Wang, and D. Pye, "Determination of the modulus of elasticity of the human cornea," *Journal of refractive surgery*, vol. 23, pp. 808-818, 2007.

[7] B. Coudrillier, J. Tian, S. Alexander, K. M. Myers, H. A. Quigley, and T. D. Nguyen, "Biomechanics of the Human Posterior Sclera: Age-and Glaucoma-Related Changes Measured Using Inflation TestingScleral Biomechanical Changes with Age/Glaucoma," *Investigative ophthalmology & visual science*, vol. 53, pp. 1714-1728, 2012.

[8] J. C. Lacal, R. Perona, and J. Feramisco, *Microinjection*: Springer Science & Business Media, 1999.

[9] D. B. Burr and M. R. Allen, *Basic and applied bone biology*: Academic Press, 2013.

[10] I. University of California and O. o. Research, "DNA Microinjection Services," ed, 2015.

[11] R. D. Goldman, D. L. Spector, and A. C. Swedlund, *Live cell imaging: a laboratory manual*: Cold Spring Harbor Laboratory Press Cold Spring Harbor, NY:, 2005.

[12] Narishige. (2016). *IM-6 Microinjector*. Available: http://products.narishige-group.com/group1/IM-6/injection/english.html

[13] Narishige. (2016). *IM-11-2*. Available: http://products.narishige-group.com/group1/IM-11-2/injection/english.html

[14] I. Tritech Research. (2016). *MINJ-D*. Available: http://www.tritechresearch.com/MINJ-D.html

[15] Eppendorf. (2016). *FemtoJet® 4i and FemtoJet® 4x*. Available: https://online-shop.eppendorf.com/OC-en/Cell-Manipulation-44522/Microinjection-44526/FemtoJet4i-and-FemtoJet4x-PF-67155.html

[16] D. W. McRobbie, E. A. Moore, M. J. Graves, and M. R. Prince, *MRI from Picture to Proton*: Cambridge university press, 2007.

[17] Z. T. H. Tse, H. Elhawary, M. Rea, B. Davies, I. Young, and M. Lamperth, "Haptic needle unit for MR-guided biopsy and its control," *Mechatronics, IEEE/ASME Transactions on,* vol. 17, pp. 183-187, 2012.

[18] K. Chinzei, R. Kikinis, and F. A. Jolesz, "MR compatibility of mechatronic devices: design criteria," in *Medical Image Computing and Computer-Assisted Intervention–MICCAI'99*, 1999, pp. 1020-1030.

[19] M. Skopec, "A Primer on Medical Device Interactions with Magnetic Resonance Imaging Systems, Feb. 4, 1997, CDRH Magnetic Resonance Working Group, US Department of Heatlh and Human Services," *Food and Drug Administration, Center for Devices and Radiological Health, Updated May*, vol. 23, p. 17, 1997.

[20] H. Sajima, H. Kamiuchi, K. Kuwana, T. Dohi, and K. Masamune, "MR-safe pneumatic rotation stepping actuator," *Journal of Robotics and Mechatronics*, vol. 24, pp. 820-827, 2012.

[21] D. Stoianovici, A. Patriciu, D. Petrisor, D. Mazilu, and L. Kavoussi, "A new type of motor: pneumatic step motor," *Mechatronics, IEEE/ASME Transactions on*, vol. 12, pp. 98-106, 2007.

[22] K. Chinzei and K. Miller, "Towards MRI guided surgical manipulator," *Medical science monitor*, vol. 7, pp. 153-163, 2001.

[23] C. Bergeles, P. Vartholomeos, L. Qin, and P. E. Dupont, "Closed-loop commutation control of an MRI-powered robot actuator," in *Robotics and Automation (ICRA), 2013 IEEE International Conference on*, 2013, pp. 698-703.

[24] Y. Wang, H. Su, K. Harrington, and G. S. Fischer, "Sliding mode control of piezoelectric valve regulated pneumatic actuator for MRI-compatible robotic intervention," in *ASME 2010 Dynamic Systems and Control Conference*, 2010, pp. 23-28.

[25] Y. Chen, K.-W. Kwok, and Z. T. H. Tse, "An MR-Conditional High-Torque Pneumatic Stepper Motor for MRI-Guided and Robot-Assisted Intervention," *Annals of biomedical engineering*, vol. 42, pp. 1823-1833, 2014.

[26] Y. Chen, C. D. Mershon, and Z. T. H. Tse, "A 10-mm MR-Conditional Unidirectional Pneumatic Stepper Motor," *IEEE Trans Mech*, 2015.

[27] Y. Wei, Y. Chen, Y. Yang, and Y. Li, "Novel Design and 3D Printing of Non-Assembly Controllable Pneumatic Robots."

[28] S. Bhavikatti and K. Rajashekarappa, *Engineering Mechanics*: New Age International, 1994.

[29] A. Wineland, Y. Chen, and Z. T. H. Tse, "Magnetic Resonance Imaging Compatible Pneumatic Stepper Motor With Geneva Drive," *Journal of Medical Devices,* vol. 10, p. 020950, 2016.

[30] M. A. Tavallaei, P. M. Johnson, J. Liu, and M. Drangova, "Design and evaluation of an MRI-compatible linear motion stage," *Medical physics,* vol. 43, pp. 62-71, 2016.

[31] J. Nofiele, Q. Yuan, M. Kazem, K. Tatebe, Q. Torres, A. Sawant, *et al.*, "An MRI-compatible platform for one-dimensional motion management studies in MRI," *Magnetic resonance in medicine,* 2015.

[32] S. M. I. Technologies, "MRI Compatible Multi-Modality Motion Stage," ed. www.simultec.com: Shelley Medical Imaging Technologies, p. 1.

[33] H. Apparatus. (2016). *MRI Compatible Syringe Pump*. Available: http://www.harvardapparatus.com/pumps-liquid-handling/syringe-pumps/mri-compatible-syringe-pump/mri-compatible-syringe-pump.html

[34] Chemyx. (2016). *NanoJet MRI Syringe Pump*. Available: https://www.chemyx.com/syringe-pumps/nanojet/

[35] A. International, "ASTM F2503-13, Standard Practice for Marking Medical Devices and Other Items for Safety in the Magnetic Resonance Environment," ed: ASTM International, 2013.

APPENDICES

A. Control Box Wiring Schematic

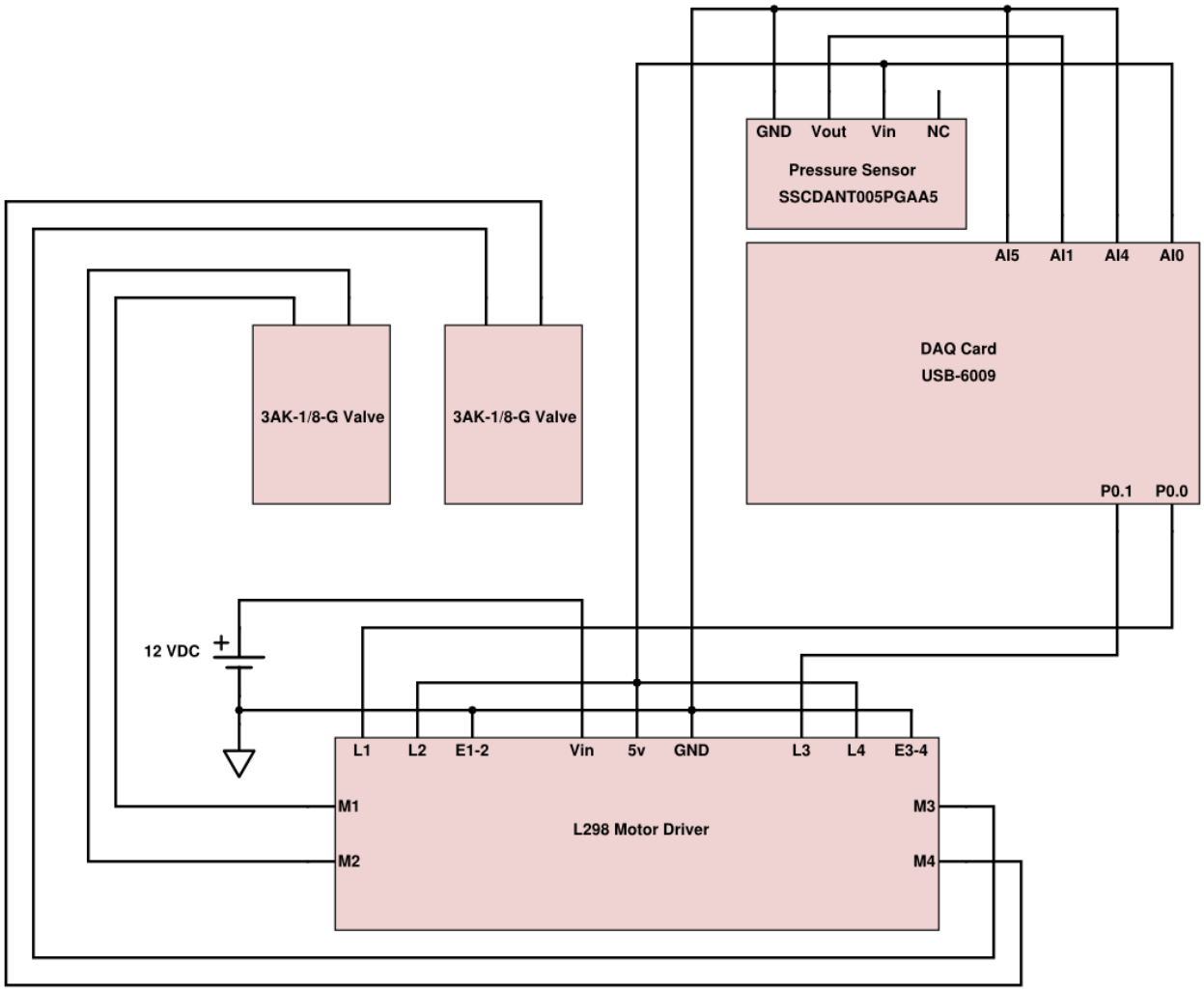

Figure A.1: Above is the wiring diagram of the control box. The components are arranged similarly to their respective positions inside the control box.

B. Microinjector LabVIEW Code

The program, also known as a virtual instrument (VI), uses state machine designs to control the microinjector and monitor pressure, volume, and displacement parameters while logging the parameters to an external file. The principle state machine contains three states. The first state initializes the configuration file. The configuration file contains two parameters: syringe size and displacement of the carriage. If a configuration file has not been created, the VI creates one with the syringe size set to *small* and the displacement set to zero. Otherwise, the VI reads in the parameters of the previous syringe size and displacement.

The second state of the principle state machine contains the majority of the program; it includes the controls for the microinjector, while loops to monitor various parameters, and the data logging function. The Control Mode while loop contains seven different modes: Standby, Auto Seek Pressure, Auto Seek Volume, Inject One Step, Retract One Step, Fully Retract, and All Stop. Some control modes utilize the stepper motor which is controlled by a subVI during advance/retract states. The subVI for the stepper motor is shown in Figure B.1. The subVI doubles the number of steps required for injection or retraction to create iterations for a for-loop. For even-numbered iterations, a digital high signal is sent to one of the pneumatic valves in the control box for a specified amount of time. For odd-numbered iterations, a digital low signal is sent to turn off the valve. Therefore, an even-numbered iteration and its consecutive odd-numbered iteration form one period, which is one step of the stepper motor.

Standby is the default mode and is initiated when the VI is executed. Also, Standby is selected after other modes have finished their cycles. During Standby, the System Operation indicator displays “Standing By”, and the System Messages and Errors indicator displays the most recent system message. If there is no system message, the indicator displays “No Errors”.

The Auto Seek Pressure mode injects or retracts the syringe until the desired pressure is achieved. If the desired pressure is lower than the applied pressure, then the system will retract the syringe until the applied pressure becomes less than the desired pressure. Once this is achieved the system will inject the syringe until the applied pressure is greater than or equal to the desired pressure. Both injection and retraction of the syringe are controlled by a state machine. If the option to maintain pressure is set to true, the Control Mode will stay in Auto Seek Pressure mode until the option is unchecked. Auto Seek Pressure with Maintain Pressure enabled will also stop if Standby or All Stop is selected. During Auto Seek Pressure, the System Operation indicator displays "Auto Seek Pressure: Injecting" if the device is injecting and "Auto Seek Pressure: Retracting" if retracting. If the displacement count is zero, the system cannot retract, and an error message is displayed. Then the system goes to Standby. Likewise, if displacement count is at maximum for the syringe, the system cannot inject, and an error message is displayed. The system then resorts to Standby.

Auto Seek Volume can be utilized for injection only. The displacement is multiplied by the amount of volume per step of the selected syringe size. During Auto Seek Volume, the System Operation indicator displays "Auto Seek Volume: Injecting". Once the desired volume has been displaced, the system resorts to Standby. If the carriage has reached a maximum before reaching the desired pressure, an error message is displayed, and the system resorts to Standby.

Inject One Step and Retract One Step are simple modes that use state machines. Each starts by checking the current displacement. If there is space to inject or retract, the state is changed to advance or retract the motor, respectively. Otherwise, a system message is displayed indicating that the linear guide is fully injected or fully retracted.

Fully Retract is also controlled by a state machine. If there is room to retract, the motor retracts the syringe automatically until displacement reaches zero. Otherwise, a system message is displayed indicating that the linear guide is fully retracted. The Fully Retract mode can be cancelled by activating either Standby or All Stop.

All Stop ends the second state of the principle state machine. When All Stop is selected, the stop button of the Control Mode's while loop is set to true. At the same time, the system status displays "All Stopped", and the stop buttons of all other while loops inside the second state of the principle state machine are set to true. Then the second state ends, and the VI continues to the third and final state of the principle state machine.

The pressure sensor while loop contains a subVI that calculates the applied pressure by using the transfer function found in the sensor's datasheet. The while loop for the pressure sensor is shown in Figure B.2. And the subVI for the pressure sensor is shown in Figure B.3. To acquire the data, both the number of samples and sample rate are set to 100. The data is written to a local variable to be used throughout the rest of the VI's operation. To stop the while loop, the Control Mode must be equal to All Stop.

The data logging while loop saves values such as pressure, volume, displacement, system operation status, system messages and errors, and the time of save. The amount of time between saved data points can be changed, but the default number is 30 seconds. An Elapsed Time VI manages the time between data points and monitors the date and time for the logged data. The Control Mode must be set to All Stop in order to stop the data logging while loop. Figure B.4 shows the while loop for the data logging function.

After pressing All Stop, the VI enters the third state of the principle state machine. The third state of the principle state machine overwrites the configuration file with new syringe size

and displacement data and ends the VI. When the VI is executed again, the VI displays the previous configuration of the system.

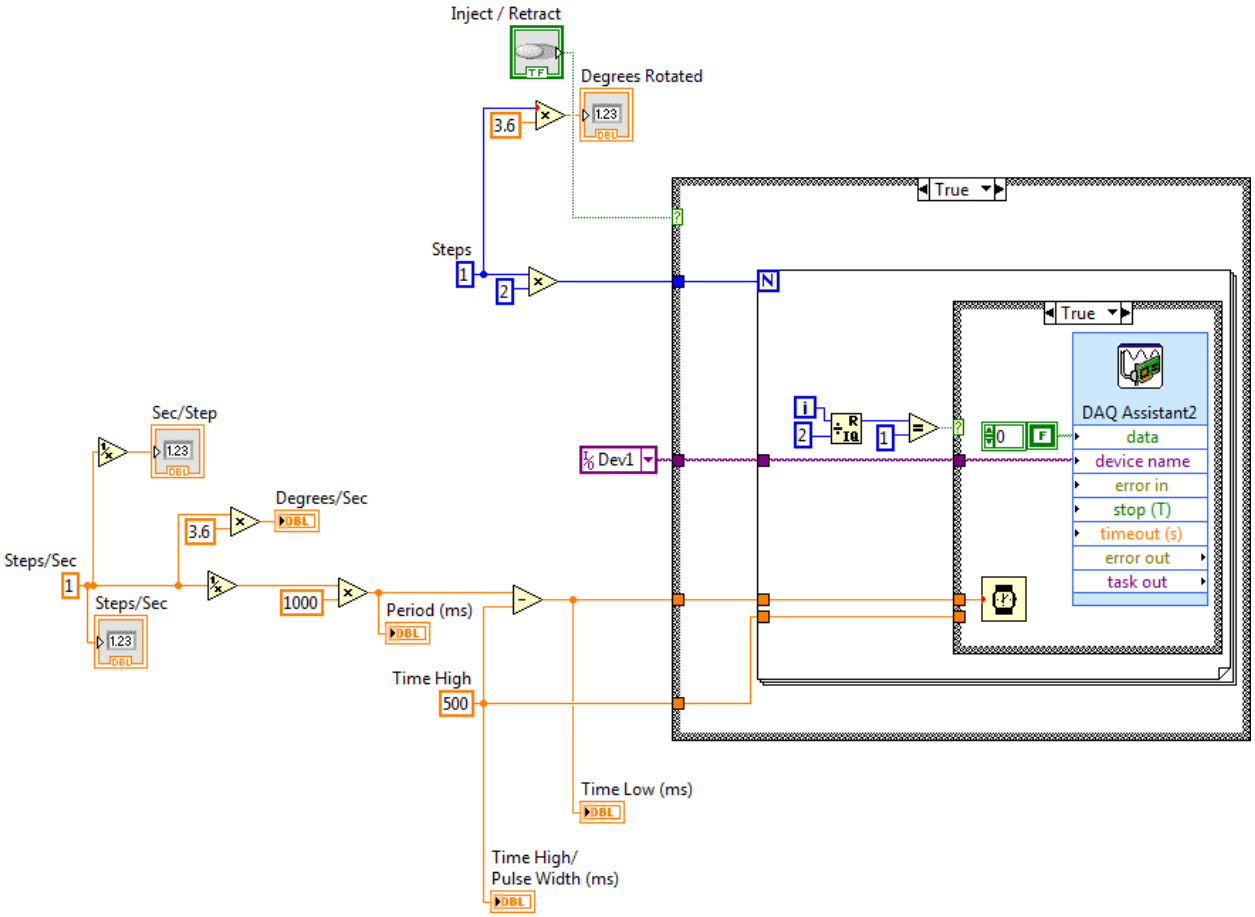

Figure B.1: The subVI for controlling the stepper motor

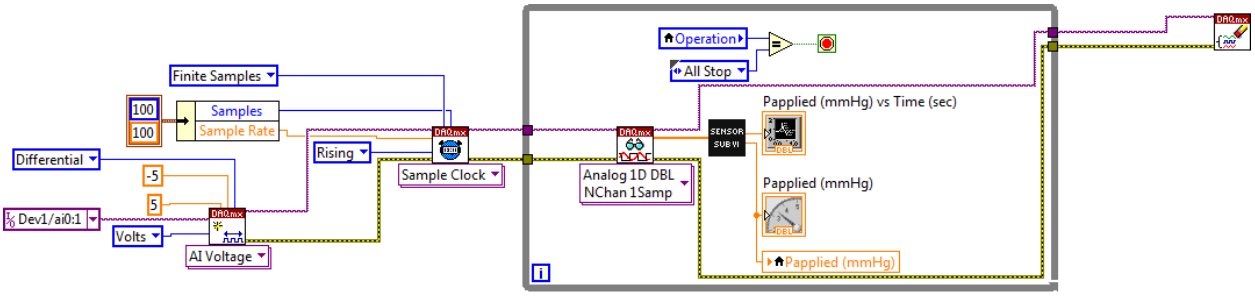

Figure B.2: This sub-function initiates and runs the pressure sensor subVI.

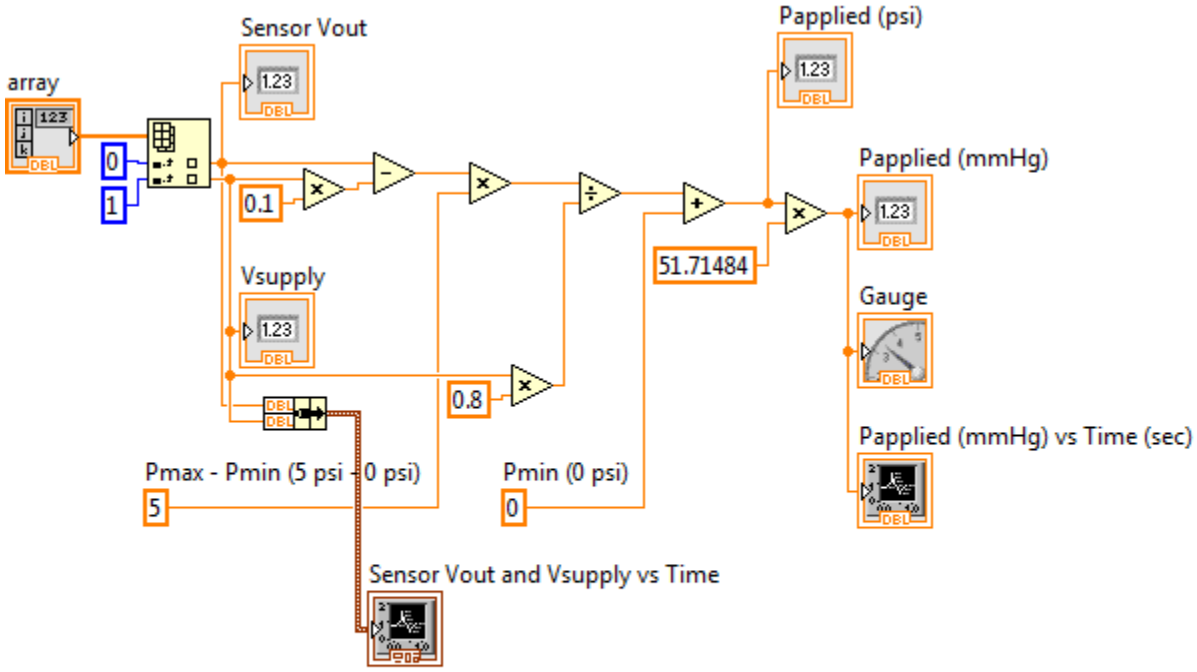

Figure B.3: The subVI for the pressure sensor along with the transfer function solved for applied pressure (Papplied)

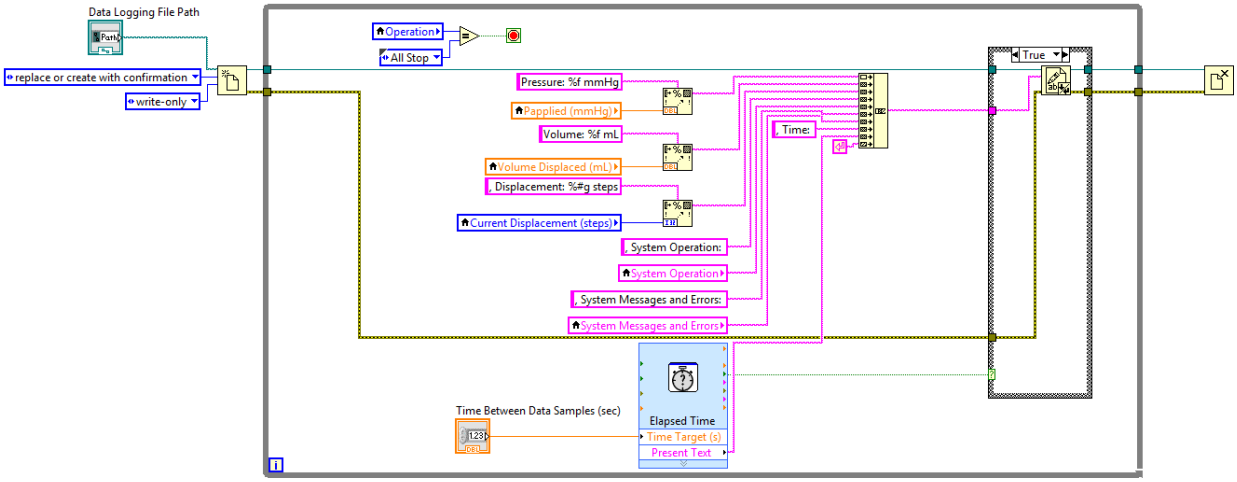

Figure B.4: The while loop for the data logging function